Development/Plasticity/Repair

Somatotopy of Mouse Spinothalamic Innervation and the Localization of a Noxious Stimulus Requires Deleted in Colorectal Carcinoma Expression by Phox2a Neurons

Shima Rastegar-Pouyani,[1,2] **Timothy E. Kennedy,**[2,3] **and Artur Kania**[1,2,4,5]

[1]Institut de Recherches Cliniques de Montréal, Montréal Québec H2W 1R7, Canada, [2]Integrated Program in Neuroscience, McGill University, Montréal Québec H3A 2B4, Canada, [3]Department of Neurology & Neurosurgery, Montreal Neurological Institute, McGill University, Montréal Quebéc H3A 2B4, Canada, [4]Division of Experimental Medicine, McGill University, Montréal Québec H3A 2B2, Canada, and [5]Department of Anatomy and Cell Biology, McGill University, Montréal QC H3A 0C7, Canada

Anterolateral system (AS) neurons transmit pain signals from the spinal cord to the brain. Their morphology, anatomy, and physiological properties have been extensively characterized and suggest that specific AS neurons and their brain targets are concerned with the discriminatory aspects of noxious stimuli, such as their location or intensity, and their motivational/emotive dimension. Among the recently unraveled molecular markers of AS neurons is the developmentally expressed transcription factor Phox2a, providing us with the opportunity to selectively disrupt the embryonic wiring of AS neurons to gain insights into the logic of their adult function. As mice with a spinal-cord-specific loss of the netrin-1 receptor deleted in colorectal carcinoma (DCC) have increased AS neuron innervation of ipsilateral brain targets and defective noxious stimulus localization or topognosis, we generated mice of either sex carrying a deletion of *Dcc* in Phox2a neurons. Such Dcc^{Phox2a} mice displayed impaired topognosis along the rostrocaudal axis but with little effect on left-right discrimination and normal aversive responses. Anatomical tracing experiments in Dcc^{Phox2a} mice revealed defective targeting of cervical and lumbar AS axons within the thalamus. Furthermore, genetic labeling of AS axons revealed their expression of DCC on their arrival in the brain, at a time when many of their target neurons are being born and express *Ntn1*. Our experiments suggest a postcommissural crossing function for netrin-1:DCC signaling during the formation of somatotopically ordered maps and are consistent with a discriminatory function of some of the Phox2a AS neurons.

Key words: **anterolateral system; DCC; development; nociception; Phox2a; topognosis**

Significance Statement

How nociceptive (pain) signals are relayed from the body to the brain remains an important question relevant to our understanding of the basic physiology of pain perception. Previous studies have demonstrated that the AS is a main effector of this function. It is composed of AS neurons located in the spinal cord that receive signals from nociceptive sensory neurons that detect noxious stimuli. In this study, we generate a genetic miswiring of mouse AS neurons that results in a decreased ability to perceive the location of a painful stimulus. The precise nature of this defect sheds light on the function of different kinds of AS neurons and how pain information may be organized.

Introduction

The sensation of a noxious stimulus (nociception) involves the appreciation of its discriminatory aspects such as location, intensity, and modality, as well as its emotive and motivational dimension driving the nocifensive response that eventually counters the stimulus (Price and Dubner, 1977). Many insights into the neuronal mechanisms of nociception came from anatomic and physiological characterization of spinal projection neurons at the origin of the anterolateral system (AS). Their function is the relay of signals from peripheral nociceptive sensory neurons to various brain targets such as the parabrachial (PB) nucleus, periaqueductal gray (PAG), and the thalamus (Lima, 2008). Proposed AS neuron functions reflect the multifaceted nature of pain; those

Received June 13, 2022; revised Aug. 7, 2022; accepted Aug. 9, 2022.

Author contributions: A.K. and S.R-P. designed research; S.R-P. performed research; S.R-P. and T.E.K. contributed unpublished reagents/analytic tools; A.K., S.R-P., and T.E.K. analyzed data; and A.K. and S.R-P. wrote the paper

S.R-P. was supported by McGill University Healthy Brains, Healthy lives and a Transat Scholarship to the Fondation Institut de Recherches Cliniques de Montréal, and A.K. was supported by operating and project grants from the Canadian Institutes of Health Research (PJT-162225, MOP-77556, PJT-153053, and PJT-159839). We thank Manon Laprise and Farin B. Bourojeni for assistance with adeno-associated virus anterograde labeling, Meirong Liang for mouse genotyping, Kevin Sangster and Melissa Pestemalciyan for assistance with tissue processing, Dominic Fillion for technical assistance with confocal microscopy, Jean-François Brunet for providing the Phox2a antibody, and R. Brian Roome and Kevin Sangster for feedback and comments on the manuscript.

The authors declare no competing financial interests.

Correspondence should be addressed to Artur Kania at artur.kania@ircm.qc.ca.

https://doi.org/10.1523/JNEUROSCI.1164-22.2022

occupying the superficial dorsal horn of the spinal cord (AS^{Sup}) have been associated with the discriminative dimension of pain, whereas those residing in deeper layers of the dorsal horn and the lateral spinal nucleus (AS^{Deep}) have been associated with other aspects of pain such as its emotive-motivational dimension (Ribeiro-da-Silva and De Koninck, 2008; Todd, 2010). One feature of AS^{Sup} neurons consistent with their proposed localization function is their predominantly contralateral brain target innervation, raising the possibility that the developmental manipulation of this topography might provide specific insights into their discriminative function.

Generally, contralaterally innervating spinal neurons project their axons through the ventral spinal commissure, which forms during embryogenesis by decussating growth cones responding to axon guidance cues that attract or repel them from the spinal midline (Comer et al., 2019). One such signal is netrin-1, whose presence at the spinal midline is detected by the receptor deleted in colorectal carcinoma (DCC) and promotes commissural crossing (Kennedy et al., 1994; Serafini et al., 1996; Fazeli et al., 1997). Our previous work revealed that mice with a spinal-cord-specific knock-out of *Dcc* (Dcc^{SpC}) have an increased incidence of AS axons innervating the ipsilateral thalamus, PB, and PAG (Bourojeni et al., 2021). Such mice, and humans with mutations in the *DCC* gene, have impaired left-right localization of noxious stimuli, but the specific identity of the connections affected has remained unclear (Da Silva et al., 2018). Several studies unraveled the molecular characteristics of AS neurons opening a way for their more precise functional manipulation (Huang et al., 2019; Choi et al., 2020; Wercberger et al., 2021). Within the spinal cord, the transcription factor Phox2a is developmentally expressed in the two principal populations of AS neurons while being absent from locally projecting spinal interneurons. Phox2a expression reveals an intriguing developmental diversity of birth timing, soma migration, and molecular specification of AS^{Sup} and AS^{Deep} neurons. Furthermore, a developmental knock-out of *Phox2a* in the spinal cord results in the loss of innervation of at least one AS brain target and decreased nocifensive responses, implying a function of AS neurons in the relay of nociceptive signals from the spinal cord to the brain (Roome et al., 2020). Based on these observations, we aimed to disrupt the laterality of AS neuron connections via a Phox2a AS neuron-specific *Dcc* knock-out. Here, we describe a specific impairment in stimulus localization of such mutants. The anatomy of their AS connections as well as the developmental timeline of AS axons reveal a surprising role for DCC in the development of neuronal connections concerned with noxious stimulus localization along the rostrocaudal axis.

Materials and Methods

Mouse colony management and maintenance

Mice of either sex were used in this study. All animal handling protocols were reviewed and approved by the Animal Care Committee of the Institut de Recherches Cliniques de Montréal. Adult mice were 11–17 weeks old at the start of the experiments and were maintained on a 12 h light/dark cycle in cages with a maximum cage capacity of five mice with food and water *ad libitum*.

Generation of mice and embryos

The following transgene combinations were generated: $Phox2a^{Cre}$; $Dcc^{f/f}$, $Phox2a^{Cre}$, $Dcc^{f/+}$, $Dcc^{f/f}$, $Ntn1^{Bgeo}$ and $Phox2a^{Cre}$; $Cdx2^{FlpO}$; $R26^{FSF\text{-}LSL\text{-}tdT}$ by breeding mice carrying one or more of the required alleles/transgenes. Detailed transgenic line information is in Table 1. Genotyping of mouse tail DNA samples was done by PCR with primers for Dcc^{f} and Dcc^{+} alleles, as well as *Cre, FlpO,* $R26^{FSF\text{-}LSL\text{-}tdT}$, and *lacZ* (*Bgeo*) as previously described (Skarnes et al., 1995; Madisen et al., 2010; Krimpenfort et al., 2012; Abraira et al., 2017; Roome et al., 2020). To generate embryos of specific developmental ages, the presence of a vaginal plug at 6:00 A.M. defined the embryonic day (E)0.5.

Tissue preparation

Embryos were harvested after anesthetizing the mother with 0.4 ml ketamine/xylazine (10 mg/ml Ketamine [100 mg/ml, drug identification number (DIN) 02374994, Code = 440893, Vetoquinol], 1 mg/ml Xylazine (100 mg/ml, DIN 02450240, Dechra Veterinary Products) in 0.9% saline followed by cervical dislocation and dissected in 1× PBS (catalog #BP399, Fisher Scientific) at 4°C, transferred to 4% paraformaldehyde (PFA) solution, and left to fix for 2 h while shaking at 4°C. After fixation, embryos were rinsed in 1× PBS, kept in cryoprotection solution (30% sucrose in 1× PBS) in 4°C until they sank, and were trimmed for mounting in Tissue-Tek optimal cutting temperature compound (catalog #4583, VWR) before cryosectioning.

Adult mice were transcardially perfused with 15 ml of 0.9% saline (9 g of NaCl in 1000 ml H_2O filtered by a Milli-Q Ultrapure system) followed with 15 ml of 4% PFA. Dissected brain and spinal cord were rinsed with 1× PBS and kept in PFA fixative for 1 h at 4°C while shaking. These were washed again with 1× cold PBS and equilibrated in 30% sucrose solution at 4°C. Tissues were cut into 25 μm sections for all experiments using a Cryostar NX70 cryostat (Thermo Fisher Scientific).

Immunostaining and in situ *mRNA detection*

Sections were washed three times for 5 min with 1× PBS at room temperature. Then a blocking solution containing 5% heat-inactivated normal horse serum (catalog #119K0364, Millipore Sigma) in 1× PBS containing 0.1% Triton X-100 (catalog #9002-93-1, Fisher Scientific) was gently applied to the sections and incubated for 30 min at room temperature. Next, slides were incubated with primary antibodies (Table 1) overnight at 4°C. On the next day, slides were rinsed three times with PBS and incubated with fluorophore-conjugated secondary antibodies for 2 h at room temperature. After incubation, slides were washed and coverslipped with 10% MOWIOL (catalog #81381, MilliporeSigma) and 25% glycerol (catalog #56-81-5, MilliporeSigma) in MilliQ water. Slides were kept at room temperature until dry and then at 4°C until imaging. To detect netrin-1 protein, antigen retrieval was performed before immunostaining: slides were postfixed with 4% PFA for 10 min and rinsed with PBS three times for 5 min each. Sodium citrate buffer containing 0.05% Tween 20 (catalog #9005-64-5, MilliporeSigma), pH 6.0, was brought to a boil on a bench-top heater, and the slides were incubated in the boiling buffer for 2.5 min. Slides were allowed to cool in the buffer solution for 20 min at room temperature, rinsed three times for 5 min each, and processed for immunohistochemistry as above.

For *in situ* mRNA hybridization, *Ntn1* amplification primers (Forward: CTTCCTCACCGACCTCAATAAC and Reverse: GGTAATACGACTCA CTATAGGGTAGAGCTCCATGTTGAATCTGC) were designed using Primer3 version 0.4.0 software (Rozen and Skaletsky, 2000), with the reverse primer containing the T7 polymerase promoter. One-step RT-PCR (Mastercycler nexus GX2, Eppendorf) was performed using T7 polymerase (Invitrogen) to make a cDNA template from E11.5 mouse pooled brain RNA. The PCR product was purified by gel electrophoresis in 1% agarose gel and extracted from the gel using QIAquick Gel Extraction Kit (catalog #28706X4, Qiagen). The purified DNA was then reamplified by PCR. The yield of DNA was estimated by the Low DNA Mass Ladder (Invitrogen) after gel electrophoresis. DIG-labeled RNA probes were synthesized by *in vitro* transcription with T7 RNA polymerase using a DIG RNA labeling kit (catalog #11175025910, Roche). The *Ntn1* probe was verified by sequencing.

Stereotaxic injection of retrograde tracers

Three to four hours before the surgery, mice received 1 mg/kg buprenorphine for analgesia. A mixture of 5% isoflurane (catalog #CP0406V2, Fresenius Kabi) in oxygen was used to anesthetize the mice, and the isoflurane level was set at 2.5% in oxygen during the operation. Eye ointment was applied to the eyes to keep them moist. The top of the head

Table 1. Resources and reagents used

Reagent or resource	Source/reference	Identifier
Mice (MGI notation)		
Dcc^{flox}	Krimpenfort et al. 2012	MGI: 3665466
Phox2a^{Cre}	Roome et al. 2022	RRID: NA
Ai14	The Jackson Laboratory	Catalog #JAX:007908
B6;129S6-Gt (ROSA)26Sortm14(CAG- tdTomato) Hze/J		RRID:IMSR_JAX:007908
Cdx2^{FlpO}	Dr. Martyn Goulding, Salk Institute, San Diego	MGI: 5911680
Tg(CDX2-flpo)#Gld		RRID: NA
Ai65	The Jackson Laboratory	Catalog #JAX:021875
B6;129S-Gt ROSA)26Sortm65.1(CAG- dTomato) Hze/J		RRID:IMSR_JAX:021875
Ntn1^{Bgeo}	Skarnes et al., 1995	RRID: NA
129S1/SvImJ	The Jackson Laboratory	Catalog #JAX:002448
		RRID:IMSR_JAX:002448
B6C3F1/J	The Jackson Laboratory	Catalog #JAX: 100010
		RRID:IMSR_JAX:100010
Primary antibodies		
Goat anti-mouse DCC (1:500)	R&D Systems	Catalog #AF844
		RRID:AB_2089765
Rabbit anti-Phox2a (1:10,000 from frozen stock)	Jean-François Brunet (École Normale Supérieure, Paris) (Tiveron et al., 1996)	RRID:AB_2315159
Rabbit anti-RFP (red fluorescent protein; 1:1000)	Rockland	Catalog #600-401-379
		RRID:AB_2209751
Goat anti-tdT (red fluorescent protein; 1:300)	SICGEN	Catalog #AB8181-200
		RRID:AB_2722750
Rabbit anti-GFP (1:1000)	Life Technologies	Catalog #A-11122
		RRID:AB_221569
Goat anti-netrin-1 (1:200)	R&D Systems	Catalog #AF1109,
		RRID:AB_2298775
Rabbit anti-c-*fos* (1:500)	Cell Signaling Technology	Catalog #2250S
		RRID:AB_2247211
Rabbit anti-Pax6 (1:500)	Millipore	Catalog #AB2237,
		RRID:AB_1587367
Rabbit anti-Sox2 (1:200)	Abcam	Catalog #97959
		RRID:AB_2341193
Secondary antibodies		
Alexa 488 Donkey anti-Rabbit (1:500)	Jackson ImmunoResearch Laboratories	Catalog #711–545-152
		Lot #141848
		RRID:AB_2313584
Alexa 488 Donkey anti-Goat (1:500)	Jackson ImmunoResearch Laboratories	Catalog #705–545-147
		Lot #136089
		RRID: AB_2336933
Cy3 Donkey anti-Rabbit (1:500)	Jackson ImmunoResearch Laboratories	Catalog #711–165-152
		Lot #138270
		RRID:AB_2307443
Cy3 Donkey anti-Goat (1:500)	Jackson ImmunoResearch Laboratories	Catalog #705–165-147
		Lot #134527
		RRID:AB_2307351
Cy5 Donkey anti-Rabbit (1:500)	Jackson ImmunoResearch Laboratories	Catalog #711–175-152
		Lot #138336
		RRID: AB_2340607
Cy5 Donkey anti-Goat (1:500)	Jackson ImmunoResearch Laboratories	Catalog #: 705–175-147 Lot#: 134531
		RRID:AB_2340415
Chemicals		
(*E*)-Capsaicin	Tocris Bioscience	Catalog #0462
		Lot #7A/218361
		RRID: NA
4′,6-diamidino-2-phenylindole (DAPI)	Thermo Fisher Scientific	Catalog #D1306
		RRID: NA
Alexa 488-conjugated Choleratoxin B	Thermo Fisher Scientific	Catalog #C22841
		Lot #2038245
		RRID: NA
X-gal	Millipore Sigma	Catalog #7240-90-6
		RRID: NA
MOWIOL	Millipore Sigma	Catalog #81381
		RRID: NA

MGI, Mouse Genome Informatics; NA, Not applicable.

was shaved with a razor blade, and an incision was made longitudinally along the scalp to access the bregma, defined as the crossing point of two straight and perpendicular lines running along the sagittal and the coronal sutures (Geiger et al., 2008). The mouse head was stabilized in the stereotaxic frame with a digital coordinate display (catalog #940, 960, 1770, 900C, 922, 933-B, David Kopf Instruments). Coordinates adapted from the Allen Institute for Brain Science reference atlas (Lein et al., 2007) were used to target the thalamus at 1.700 mm caudal and 2.000 mm lateral from bregma, at a depth of 3.400 mm. A solution of retrograde tracer, 1% Cholera Toxin Subunit B conjugated to Alexa Fluor 488 (CTB-488; catalog #C22841, Thermo Fisher Scientific) in 1× PBS, was injected into the thalamus using the above stereotaxic apparatus via a 5 μl syringe (Hamilton) attached to an UltraMicroPump3 infuser with a Micro4 controller (World Precision Instruments). Five hundred nanoliters of the tracer were loaded into a pulled glass capillary needle attached to the syringe and injected at a rate of 100 nl/min. Following surgery, mice were monitored for infection and signs of pain for 1 week before collection of the brain and spinal cords. No animals died as a direct result of this manipulation.

Tracing and quantification of retrogradely labeled cells

Following perfusion of fixative, cryoprotection and cryosectioning, CTB-488-labeled neurons were counted in one of every four sections of the spinal cord, at C5-7 and L3–L4 levels. A total number of 10 cervical and 10 lumbar sections of 25 μm thickness were analyzed per animal. Images were captured by confocal microscope (Leica SP8) through a 20× objective, and CTB-labeled neurons were counted using the semi-manual cell counter plug-in ImageJ version 2.0.0 software. The Allen Institute for Brain Science adult mouse spinal cord atlas and the Rexed system were used to define the location of labeled neurons (Rexed, 1952; Lein et al., 2007).

Anterograde tracing of projection neurons (PNs) from spinal cord

Three to four hours before surgery, mice received 1 mg/kg buprenorphine for analgesia (slow-release buprenorphine HCl 0.6 mg/ml; catalog #RxN698382, Chiron). To anesthetize the mice, we used a mixture of 5% isoflurane in oxygen, which was reduced to 2.5% during surgery. The anesthetized mouse was placed in the stereotaxic frame (catalog #940, 960, 1770, 909C, 922, 933-B, David Kopf Instruments). Back skin was disinfected by povidone-iodine and cut to access the spinal cord with the spine held in place via ear bars. The injection was performed as in the reference protocol (Kohro et al., 2015). A 300 nl solution of adeno-associated virus (AAV)2/8-Syn-SYP1-mSOG-citrine [titer, 2.2 × 1013 genome copies (GC)/ml; lot #1385] and AAV2/8-Syn-SYP1-mSOG-mCherry (titer, 2.0 × 1013 GC/ml; lot #1410, CERVO Brain Research Center), were injected unilaterally at lumbar and cervical levels, respectively (ML, 0.45 mm; AP, 0 ± 0.5 mm; DV, 0.35 mm from the dorsal spinal midline). Two injections with 0.5 mm distance along the anterior–posterior axis were performed at each level of the spinal cord. After 4 weeks, mice were perfused with fixative, brains harvested as above and cut in the coronal plane into 25 μm sections to access ventral posterolateral thalamus (VPL), PB, and other brain areas. Axonal citrine and mCherry signals were amplified with anti-GFP and anti-RFP antibodies and localized with respect to standard anatomic features (Kohro et al., 2015). Signal quantification and overlap were assessed using ImageJ version 2.0.0 software (Schneider et al., 2012).

Mouse behavior

Capsaicin test. To assess the localization of thermal noxious stimuli, the capsaicin test was performed on eight $Phox2a^{Cre;}$ $Dcc^{f/f}$ (Dcc^{Phox2a}) and eight control littermates, which were either $Phox2a^{Cre}$, $Dcc^{f/+}$ or $Dcc^{f/f}$ mice. Mice were habituated for 30–45 min in the test chamber, which was a 10 × 10 cm Plexiglas box resting on a 25-cm-high glass platform. The mice were restrained with a towel, and a volume of 15–20 μl of 1.5 μg/20 μl capsaicin (catalog #0462, Tocris Bioscience) in DMSO solution was subcutaneously injected into the hindpaw plantar surface using a 26G3/8 needle as in the standard protocol (Sakurada et al., 1992). The mice were immediately returned to the chamber and their behavior recorded for 15 min using the video rate camera of a Galaxy A7 phone (Samsung). Raw videos were processed using Gnome software (Linux) to calculate the total licking time and time spent licking a specific paw. The output as an SRT file was processed using a Python script. Data were subjected to Student's *t* test statistical analysis using Microsoft Excel and plotted using Prism 9 (GraphPad).

Hargreaves test. Seven Dcc^{Phox2a} and six control littermate mice were placed inside 5 × 10 cm Plexiglas boxes (IITC Life Science) on top of a transparent glass platform (5 mm thick) and habituated for 30–45 min. The plantar surface of the hindpaw was stimulated by an infrared light source (catalog #PE34, IITC Life Science) at 192 W/cm^2, and withdrawal latency was recorded. To prevent tissue damage caused by radiant heat, 40 s of exposure was set as the cutoff time. The withdrawal latency was measured for each animal as the average of eight trials with a 5 min minimum interval to avoid overexposure (Hargreaves et al., 1988).

von Frey test. Mice were placed individually inside 5 × 10 cm Plexiglas boxes (IITC Life Science) set on top of a mesh surface table and habituated for 45 min. A mesh surface table was used, an easy-to-clean metal platform, with laser-cut perforations producing an open grid of 5 × 5 mm square holes allowing access to the hindpaw of the mice. Nylon filaments (Touch Test Sensory Evaluators, kits 2– 9, North Coast Medical), calibrated using a microbalance, to exert 0.015, 0.04, 0.07, 0.15, 0.44, 0.55, 1.0, and 1.3 g of force, respectively, were firmly applied to the plantar surface of the hindpaw (alternating the side of the body being tested) until they bowed for 5 s. Only withdrawal responses, evoked in an obvious manner in response to the applied stimulus, were scored (Mogil et al., 2010). The series started with filament 5 (0.15 g) and continued with increasingly thicker filaments until the first withdrawal response. Each series consisted of four trials after the first withdrawal, using a lighter filament if there was no withdrawal and a higher filament if there was withdrawal per the up-down protocol (Chaplan et al., 1994).

Conditioned place avoidance test. A conditioned place avoidance (CPA) box with two 25.5 × 20 × 20 cm conditioning chambers and a neutral central room of 15 × 20 × 20 cm, connected via 5 × 5.5 cm openings was used (Cunningham et al., 2006; Tzschentke, 2014). On the first day of testing, mice were restricted to the central room for 1 min and then allowed to freely explore the apparatus for 30 min to visit the two lateral chambers with different visual cues. On the second day, mice were allowed to freely explore the chambers for 30 min. Their movements throughout the CPA box were recorded by a top-view camera (Samsung, Galaxy A7 phone), and the recordings were processed using Gnome software (Linux) to calculate the time spent in each chamber. The chamber where the mouse spent the most time was chosen as the conditioning chamber. In the next 2 d, mice were placed in one of the conditioning chambers, and a volume of 15–20 μl of 5 μg/20 μl capsaicin (catalog #0462, Tocris Bioscience) in DMSO was subcutaneously injected into the hindpaw plantar surface. On the fifth day, mice were restricted in the central room for 1 min and allowed to freely roam the CPA box for 30 min. Time spent in chambers before and after the injection phases (second day vs the fifth day) were compared.

*c-*fos *Detection*

Expression of c-*fos* was assessed as an indicator of neuronal activity in response to nociceptive stimuli (15–20 μl of 1.5 μg/20 μl capsaicin (catalog #0462, Tocris Bioscience) in DMSO solution was subcutaneously injected into the hindpaw plantar surface. Mice were kept in their cages for 90 min after capsaicin injection, perfused, and spinal cord tissue and the whole brain were harvested. Spinal cord segments L3–L4 and brains from −4.95 mm to −5.55 mm with respect to bregma were cut into 25 μm coronal sections to assess c-*fos* immunoreactivity in the spinal cord and the PB, respectively (Hunt et al., 1987; Pilyavskii et al., 2005).

X-gal staining

X-gal solution consisting of 40 mg/ml X-gal powder (catalog #7240-90-6, MilliporeSigma) in DMSO was freshly prepared and mixed with solution A containing 1 M $MgCl_2$, 2% NP40, 2% Na-deoxycholate in 1× PBS, pH 7.2, potassium hexacyanoferrate (II) and potassium hexacyanoferrate (III) mixed at a volume ratio of 1:47:1:1, respectively). This buffer was

poured gently to cover all the slides in a slide holder in a glass receptacle. Slide holders were wrapped in aluminum foil and incubated in a 37°C water bath. Slides were periodically examined to monitor enzymatic reaction over 3–4 h. Slides were rinsed with Mili-Q water and coverslipped with the MOWIOL solution.

Microscopy and image processing

A confocal laser scanning microscope (Leica SP8) was used to capture the images. Image processing and cell count analysis were performed using ImageJ version 2.0.0 software, the cell count plug-in. The innervation area of cervical and lumbar AS axons was first normalized by pixel size in ImageJ (see Fig. 4*E*), then the innervated area was selected using the freehand selection tool in each of the 10 sections (five caudal and five rostral) per animal. The average cervical/lumbar AS axons area for each bregma level was measured in three control and 3 Dcc^{Phox2a} mice by ImageJ region of interest measure. The average innervation area in each bregma is shown as an outline, and these are stacked on top of each other in the caudal and rostral VPL.

Statistics

Quantification and statistical analysis were prepared using either Microsoft Excel or GraphPad Prism 9. All experiments were performed by a blinded researcher. Data were analyzed using paired and unpaired Student's *t* tests as well as between-subjects and mixed ANOVA, one within and one between-subject factor test. Bonferroni *post hoc* analysis was performed for data with a significant ANOVA effect. Significance is presented as $p < 0.05$, significant and not significant. The specific statistic tests performed on each dataset and exact *p* values are listed in the figure legends.

Results

Decreased accuracy of topognosis in mice with selective deletion of DCC from Phox2a-expressing neurons

We reasoned that the topognosis deficiencies caused by Dcc^{SpC} may result from an increased number of ipsilateral spinofugal AS neuron connections (Da Silva et al., 2018). To preferentially manipulate DCC expression in AS^{Sup} neurons that are likely engaged in stimulus discrimination, we took advantage of the observation that the transcription factor Phox2a is expressed by ~60% of AS^{Sup} neurons and ~30% of AS^{Deep} neurons and that the BAC (bacterial artificial chromosome) transgenic Cre recombinase driver $Phox2a^{Cre}$ is expressed in ~80% of Phox2a AS^{Sup} neurons but only in ~30% of Phox2a+ AS^{Deep} neurons. Thus, the $Phox2a^{Cre}$ driver is strongly biased for AS^{Sup} neurons, allowing access to ~50% of them in contrast to only ~10% of AS^{Deep} neurons (Roome et al., 2020; Alsulaiman et al., 2021).

We used $Phox2a^{Cre}$ and a Cre-excisable *Dcc* allele (Dcc^{f}; Krimpenfort et al., 2012) to generate two cohorts of mice, $Phox2a^{Cre}$; $Dcc^{f/f}$, abbreviated as Dcc^{Phox2a}, and control littermates carrying $Phox2a^{Cre}$, $Dcc^{f/+}$ or $Dcc^{f/f}$. To determine the efficiency and specificity with which $Phox2a^{Cre}$ induced a loss of spinal DCC expression, we focused on E10.5, when many Phox2a AS neurons are being born and at an early stage of commissural crossing (Tessier-Lavigne et al., 1988). At that age, DCC is expressed in essentially all first-born Phox2a+ neurons that eventually give rise to a large population of AS^{Sup} neurons that innervate contralateral brain targets (Roome et al., 2020). Compared with controls, $Phox2a^{Cre}$ spinal neurons consistently showed a loss of DCC expression in Dcc^{Phox2a} embryos (Fig. 1*A*; Roome et al., 2020). We also assessed the effect of Dcc^{Phox2a} on Phox2a AS neuron migration (Roome et al., 2022) and neuronal survival by producing adult Dcc^{Phox2a} mice carrying the Cre-dependent tdTomato reporter $R26^{LSL\text{-}tdT}$ (*Ai14*; Madisen et al., 2010). The number and overall location of tdTomato-expressing Phox2a AS^{Sup} and AS^{Deep} neurons did not differ between control and $Phox2a^{Cre}$ mice (Fig. 1*B*,*B'*).

We next determined the impact of DCC deletion from Phox2a neurons on the function of spinal nociceptive circuits. First, we used the Hargreaves and von Frey tests to evaluate the reflexive nocifensive responses to thermal and mechanical noxious stimuli, respectively (Hargreaves et al., 1988; Chaplan et al., 1994). Neither thermal reflex latency nor response threshold to mechanical stimulation were different between control and Dcc^{Phox2a} mice ($p = 0.15$ and $p = 0.42$, respectively; $n = 6$–7; Fig. 1*C*,*D*). Furthermore, we examined nociceptive spinal neuron activity by estimating the number of neurons expressing the activity-induced protein c-*fos* 90 min following a hindpaw injection of capsaicin, a noxious stimulus that evokes a burning sensation in humans (Hunt et al., 1987; Sakurada et al., 1992). No significant differences between control and Dcc^{Phox2a} mice were observed ($p = 0.13$; $n = 3$; Fig. 1*E*,*E'*).

We next studied Dcc^{Phox2a} mouse behaviors requiring the supraspinal transmission of nociceptive information. Thus, we injected capsaicin into one of the hind paws, a treatment that elicits robust licking of the injection site (Fig. 1*F*). The total licking time over the recorded period did not differ between Dcc^{Phox2a} and control mice, suggesting a comparable perceived stimulus intensity in Dcc^{Phox2a} and control mice (Fig. 1*G*). Next, we examined the accuracy of localizing the capsaicin injection site by normalizing the time spent licking each limb to the total licking time. Control mice spent 94.55 ± 7.71% of this time licking the injected limb and 0.26 ± 0.74%, 2.45 ± 4.12% and 2.67 ± 3.62% of time licking the contralateral hindlimb, and ipsilateral, and contralateral forelimb, respectively. In contrast, Dcc^{Phox2a} mice devoted 84.27 ± 8.9% of their licking time to the injected limb, and 0%, 9.43 ± 5.74% and 6.28 ± 4.69% to the other limbs, respectively. Statistical analysis revealed that Dcc^{Phox2a} mice spent significantly less time licking the limb injected with capsaicin and more time licking the ipsilateral forelimb ($p = 0.02$ and $p = 0.01$, respectively; Fig. 1*F*,*H*). Licking response distribution among four limb areas showed a significant difference between control and Dcc^{Phox2a} mice with the licking shifting from the injected hindpaw to ipsilateral and contralateral forepaws ($p = 0.001$; Fig. 1*I*). Time spent licking the contralateral forelimb was not significantly different between controls and Dcc^{Phox2a} mutants. These results demonstrate a decreased accuracy of localization of a noxious stimulus along the rostral-caudal axis of Dcc^{Phox2a} mutants.

Dissociation of aversive and discriminatory components of a noxious stimulus in Dcc^{Phox2a} mice

Topognosis of Dcc^{Phox2a} mutants is impaired, but the similar duration of nocifensive licking in Dcc^{Phox2a} mutants and control mice suggest that both groups appreciate the emotive/motivational dimension of this stimulus to a similar extent. To assess this difference more directly, we monitored capsaicin-evoked c-*fos* expression in the PB, an AS neuron target associated with nociceptive aversion (Bernard et al., 1996; Chiang et al., 2019; Karthik et al., 2022). To do this, we injected the plantar surface of one of the hindlimbs with capsaicin and monitored the number of c-*fos*-expressing neurons in the lateral division of the PB 90 min later. Compared with unstimulated controls, capsaicin injection evoked a marked increase in the number of c-*fos* neurons in Dcc^{Phox2a} mutant and control animals; however, this increase was not significantly different between the Dcc^{Phox2a} mutant and control groups (Fig. 2*A*,*A'*).

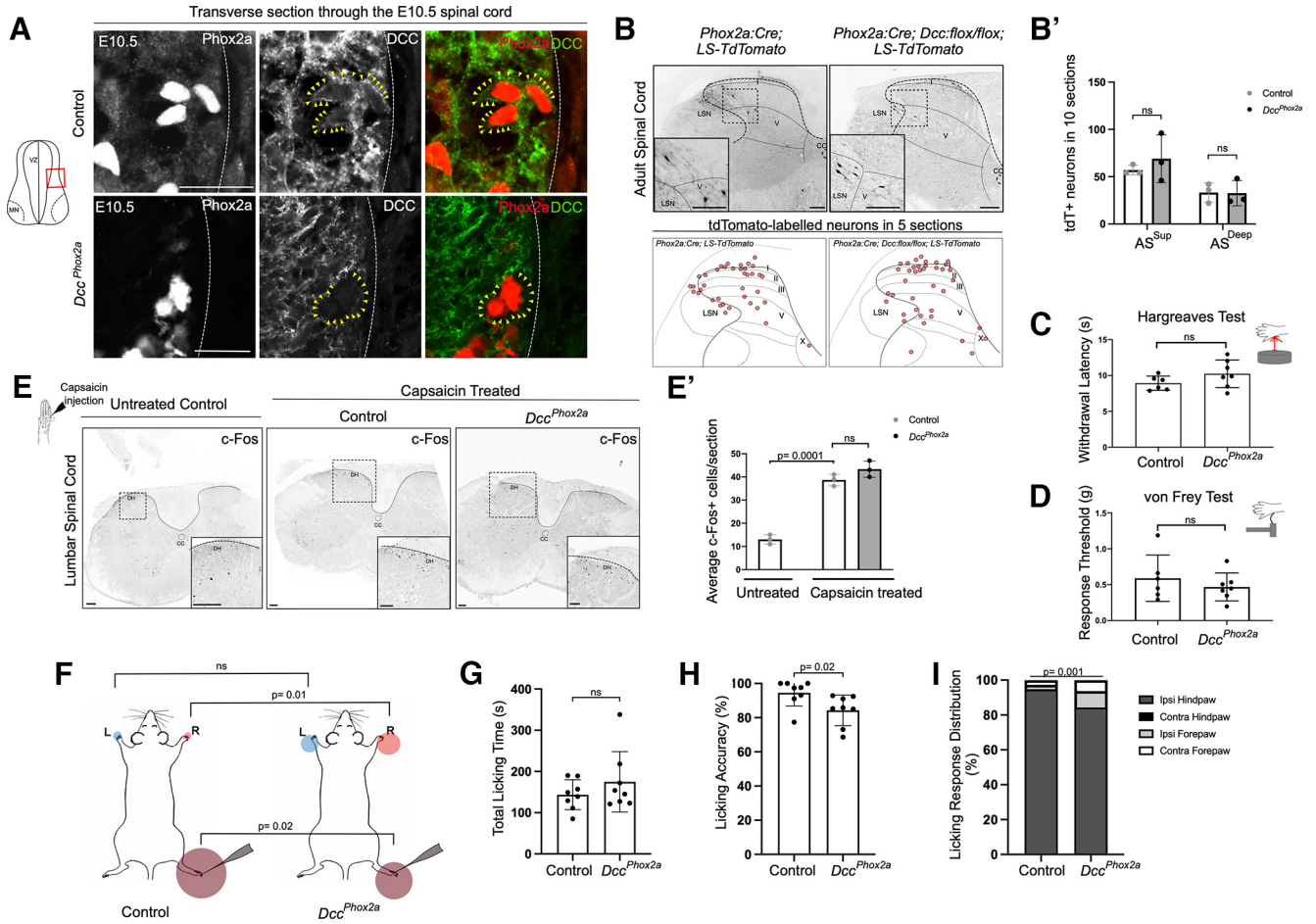

Figure 1. Decreased topognosis accuracy in mice with DCC deleted from Phox2a-expressing neurons. ***A***, Phox2a and DCC immunofluorescence in E10.5 spinal cord. Arrowheads outline DCC expression in Phox2a neuron cell bodies of control embryos and highlight DCC loss in Phox2a neurons of Dcc^{Phox2a} mutants. Images representative of $n = 3$ control and $n = 3$ Dcc^{Phox2a} embryos. Scale bar, 25 μm. ***B***, ***B'***, Phox2a neuron viability in adult Dcc^{Phox2a} model. The total number of tdT positive neurons in 10 sections of cervical spinal cord in 25-μm-thick sections (control AS^{Sup}, 57 ± 5.19%; control AS^{Deep}, 33.3 ± 10.26%; Dcc^{Phox2a} AS^{Sup}, 69 ± 25.23%; Dcc^{Phox2a} AS^{Deep}, 32.66 ± 13.31%); $n = 3$ control and $n = 3$ Dcc^{Phox2a} mice. Unpaired student's t test in ***B'***; ns, Not significant. Data indicate mean ± SD. Scale bars: 100 μm. ***C***, Withdrawal latency response to radiant heat in Hargreaves test (control, 8.92 s ± 0.99 s; Dcc^{Phox2a}, 10.24 s ± 1.92 s); $n = 6$ control and n = 7 Dcc^{Phox2a} mice. Unpaired Student's t test; ns. Data indicate mean ± SD. ***D***, Mechanical response threshold in von Frey test (control, 0.59 g ± 0.32 g; Dcc^{Phox2a}, 0.46 g ± 0.19 g); $n = 6$ control and $n = 7$ Dcc^{Phox2a} mice. Unpaired Student's t test; ns. Data indicate mean ± SD. ***E***, ***E'***, *c-fos* Expression in the dorsal horn of lumbar spinal cord after 1.5 μg/20 μl capsaicin injection in the plantar hindpaw. The average number of *c-fos*+ cells in a 25 μm section of lumbar spinal cord; $n = 3$ mice per group (untreated control, 13 ± 2; capsaicin-treated control, 38.66 ± 2.51; capsaicin-treated Dcc^{Phox2a}, 43.33 ± 3.51). Unpaired Student's t test in ***E'***; $p = 0.0001$; significant; ns. Data indicate mean ± SD. ***F***, Graphical representation of the average percentage of time spent licking each paw. Normalized by the time spent licking each paw to the total licking time; circle area is proportional to the licking time (control ipsilateral hindpaw, 94.55 ± 7.71%; control ipsilateral forepaw, 2.45 ± 4.12%; control contralateral forepaw, 2.67 ± 3.62%; Dcc^{Phox2a} ipsilateral hindpaw, 84.27 ± 8.95%; Dcc^{Phox2a} ipsilateral forepaw, 9.43 ± 5.74%; Dcc^{Phox2a} contralateral forepaw, 6.28 ± 4.69%); $n = 8$ control and $n = 8$ Dcc^{Phox2a} mice. Unpaired Student's t test; $p = 0.01$ and $p = 0.02$; significant. ***G***, ***H***, Quantification of total licking time in seconds; control, 143.62 ± 36.16; Dcc^{Phox2a}, 174.75 ± 73.3 (***G***), expressed as a fraction of the time licking the injection site (accuracy); control, 94.555 ± 7.71%; Dcc^{Phox2a}, 84.27 ± 8.95% (***H***); $n = 8$ control and $n = 8$ Dcc^{Phox2a} mice. Unpaired Student's t test; $p = 0.02$; significant; ns. Data indicate mean ± SD. ***I***, Licking response localization as a percentage of total time following capsaicin injection into one of the hindpaws (control ipsilateral hindpaw, 94.55 ± 7.71%; control contralateral hindpaw, 0.26 ± 0.74%; control ipsilateral forepaw, 2.45 ± 4.12%; control contralateral forepaw, 2.67 ± 3.62%; Dcc^{Phox2a} ipsilateral hindpaw, 84.27 ± 8.95%; Dcc^{Phox2a} contralateral hindpaw, 0%; Dcc^{Phox2a} ipsilateral forepaw, 9.43 ± 5.74%; Dcc^{Phox2a} contralateral forepaw, 6.28 ± 4.69%); $n = 8$ control and $n = 8$ Dcc^{Phox2a} mice. Mixed ANOVA, one within- and one between-subject factor, $p = 0.001$; significant. Data indicate mean ± SD.

Because the PB nucleus is only one of the brain centers involved in the processing of the aversive dimension of pain, we used a behavioral paradigm to determine the broad impact of Dcc^{Phox2a} on aversion evoked by a noxious stimulus. To do this, we turned to the CPA test in which capsaicin injections evoke aversion-based conditioning. In a modified three-chamber standard paradigm on days one and two, mice were allowed to freely explore two translucent chambers that differed in the visual cues applied to their outer surface, linked via a small neutral chamber (Cunningham et al., 2006; Fig. 2*B*). On days three and four, mice had one of their hindpaws injected with capsaicin and confined to one of the large chambers (conditioning chamber). On the testing day, mice were allowed to roam freely throughout the apparatus, and the time spent in each chamber was recorded and compared using two standard CPA scoring methods. Analysis revealed that Dcc^{Phox2a} and control mice similarly avoided the conditioning chamber ($p = 0.006$ and $p = 0.007$, respectively; Fig. 2*C*,*D*,*E*). Thus, the loss of DCC from Phox2a neurons impairs noxious stimulus topognosis but not its aversive/emotive qualities.

Increased ipsilateral innervation of the thalamus by as neurons in Dcc^{Phox2a} mice

Most mouse AS^{Sup} and many AS^{Deep} neurons are commissural neurons, preferentially innervating their brain targets on the contralateral side (Davidson et al., 2010). The impaired topognosis of Dcc^{Phox2a} mice was reminiscent of that of Dcc^{SpC} mice in which this phenotype was linked to an increased incidence of AS

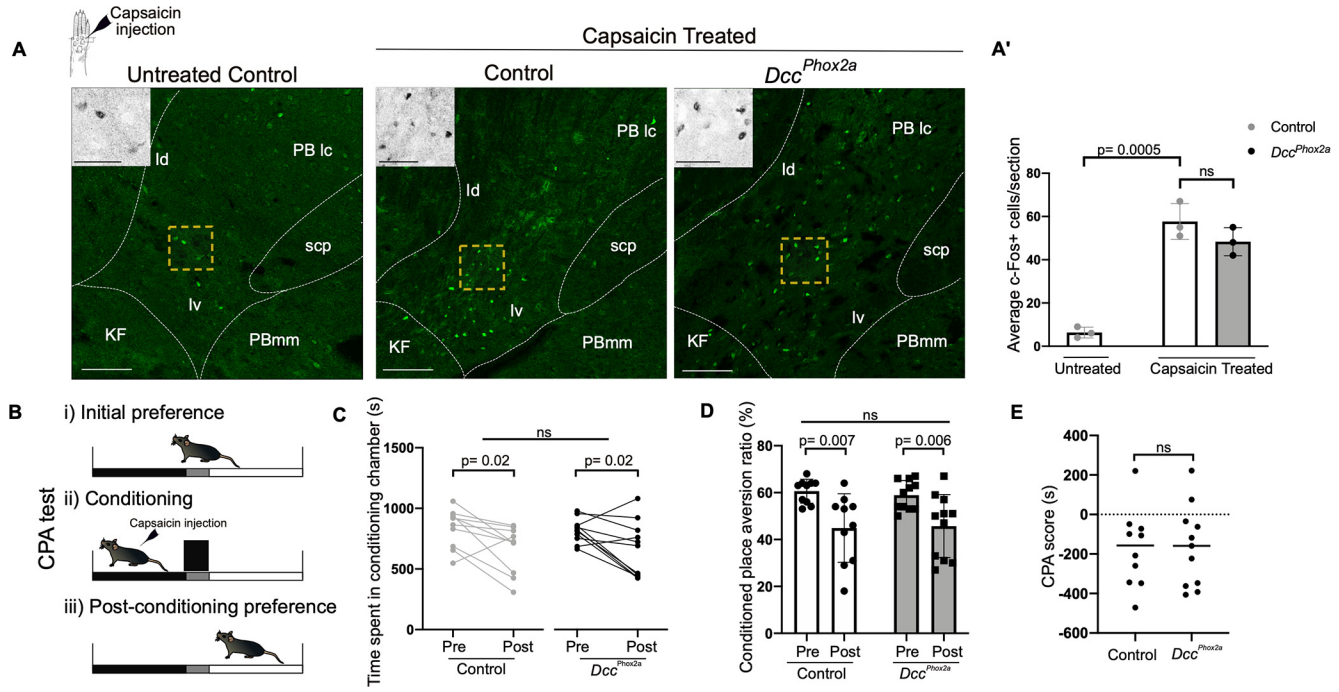

Figure 2. Normal aversive pain circuit in Dcc^{Phox2a} model. ***A***, ***A'***, c-*fos* Expression in the PB nucleus after 1.5 μg/20 μl Capsaicin injection in the plantar hindpaw. The average number of c-*fos* positive cells in a 25 μm section of the PB nucleus; $n = 3$ mice per group (untreated control, 6.33 $\pm$ 2.51; capsaicin-treated control, 57.66 $\pm$ 8.32; capsaicin-treated Dcc^{Phox2a}, 48.33 $\pm$ 6.5). Unpaired Student's *t* test in ***A'***; $p = 0.0005$; significant; ns, not significant. Data indicate mean $\pm$ SD. Scale bars: ***A***, 100 μm; insets, 25 μm. ***B***, CPA test; one side of the two-sided chamber was paired with thermal noxious stimuli by capsaicin injection. The relative percentage of time spent in the capsaicin-paired chamber preconditioning (pre) and postconditioning (post) phases was quantified in control and Dcc^{Phox2a} groups. ***C***, Time spent in capsaicin-paired chamber pre and post phases; $n = 10$ control and $n = 11$ Dcc^{Phox2a} mice (control pre, 838.2 s $\pm$ 159.34 s; control post, 664.5 s $\pm$ 193.22 s; Dcc^{Phox2a} pre, 818.18 s $\pm$ 97.39 s; Dcc^{Phox2a} post, 653.9 s $\pm$ 228.7 s). Paired Student's *t* tests were used to compare the pre/post condition in each group; $p = 0.02$; significant. Mixed ANOVA, one within- and one between-subject factor; ns. ***D***, Conditioned place aversion ratio as the fraction of time spent in the capsaicin-paired chamber pre and post phases; $n = 10$ control and $n = 11$ Dcc^{Phox2a} mice (control pre, 60.6 $\pm$ 5.12%; control post, 44.9 $\pm$ 14.59%; Dcc^{Phox2a} pre, 58.9 $\pm$ 6.25%; Dcc^{Phox2a} post, 45.72 $\pm$ 13.44%). Paired Student's *t* test to compare the pre/post condition in each group; $p = 0.007$ and 0.006; significant. Mixed ANOVA, ns. ***E***, CPA score, subtraction of time spent in capsaicin-paired chamber post from before conditioning; $n = 10$ control and $n = 11$ Dcc^{Phox2a} mice (control, -173.7 s; Dcc^{Phox2a}, -164.27 s). Unpaired student's *t* test; ns.

neurons innervating their brain targets on the ipsilateral side. Thus, we determined whether a similar shift in the laterality of AS neurons was induced in Dcc^{Phox2a} mice by labeling them with a retrograde tracer from one of their brain targets. To do this, we unilaterally injected a fluorescently conjugated Cholera Toxin B retrograde tracer into the VPL thalamus (CTB^{VPL}), and quantified the number of AS^{Sup} and AS^{Deep} neurons labeled on the ipsilateral and contralateral sides at lumbar and cervical levels (Fig. 3*A*,*B*; Roome et al., 2020). In the lumbar spinal cord, the number of CTB^{VPL}+ neurons on the ipsilateral and contralateral sides were not different between control and Dcc^{Phox2a} mice; however, at cervical levels there was a significant increase in the number of ipsilateral CTB^{VPL}+ neurons in the Dcc^{Phox2a} mice, compared with that of controls (Fig. 3*C*,*C'*). Similarly, normalizing for efficiency of tracer labeling, the ratio of ipsilateral to contralateral (I/C) CTB^{VPL}+ neurons was increased at cervical levels of Dcc^{Phox2a} mice ($p = 0.005$), but remained unchanged at lumbar levels (Fig. 3*D*,*D'*).

Next, given the discriminatory functions associated with AS^{Sup} neurons, including stimulus localization via their narrow receptive fields, we classified CTB^{VPL}+ AS neurons as AS^{Sup} and AS^{Deep} according to their laminar location. At the lumbar levels, comparing Dcc^{Phox2a} mice with controls, we did not find a significant differences in the I/C ratio of AS^{Sup} and AS^{Deep} neurons (Fig. 3*E'*,*F'*). However, at the cervical level, we observed a significant increase in the ipsilateral innervation of Dcc^{Phox2a} AS^{Sup} neurons but not of AS^{Deep} neurons (Fig. 3*E*,*F*). Given the small number of spinothalamic neurons at lumbar levels, it is possible that a laterality phenotype in Dcc^{Phox2a} mice is masked by technical variability between sections and animals. On the other hand, the loss of DCC in Phox2a neurons resulted in decreased contralateral projection of cervical AS^{Sup} neurons, consistent with a function of DCC in commissural crossing.

Impaired organization of spinothalamic innervation in Dcc^{Phox2a} mice

We next investigated the rostrocaudal organization of spinofugal projections of AS neurons by differentially labeling lumbar and cervical spinal neurons and examining their axonal projections in the PB, PAG, and thalamus, three main targets of AS neurons. To do this, we used AAVs encoding mCherry and GFP proteins fused to synaptophysin (Syn), targeting these fluorescent proteins to synaptic vesicles and thus preferentially labeling axonal termini (Oh et al., 2014). Adult Dcc^{Phox2a} and control mice were simultaneously and unilaterally injected in their cervical and lumbar spinal cords with, respectively, mCherry-Syn and GFP-Syn-encoding AAVs, and their CNS was harvested 4 weeks later and cryosectioned into 25 μm sections. Examination of infection sites revealed consistent and unilateral labeling of the dorsal horn, including superficial laminae containing AS^{Sup} neurons (Fig. 4*A*). Lumbar infections appeared more robust than cervical ones, reflecting their differential surgical accessibility. Both in Dcc^{Phox2a} and control mice, as previously, we found GFP and mCherry labeled AS axons in the PB, PAG and the thalamus, with a morphology that included varicosities ascribed to the termini of spinofugal axons in the PB and thalamus (Fig. 4*B*,*C*;

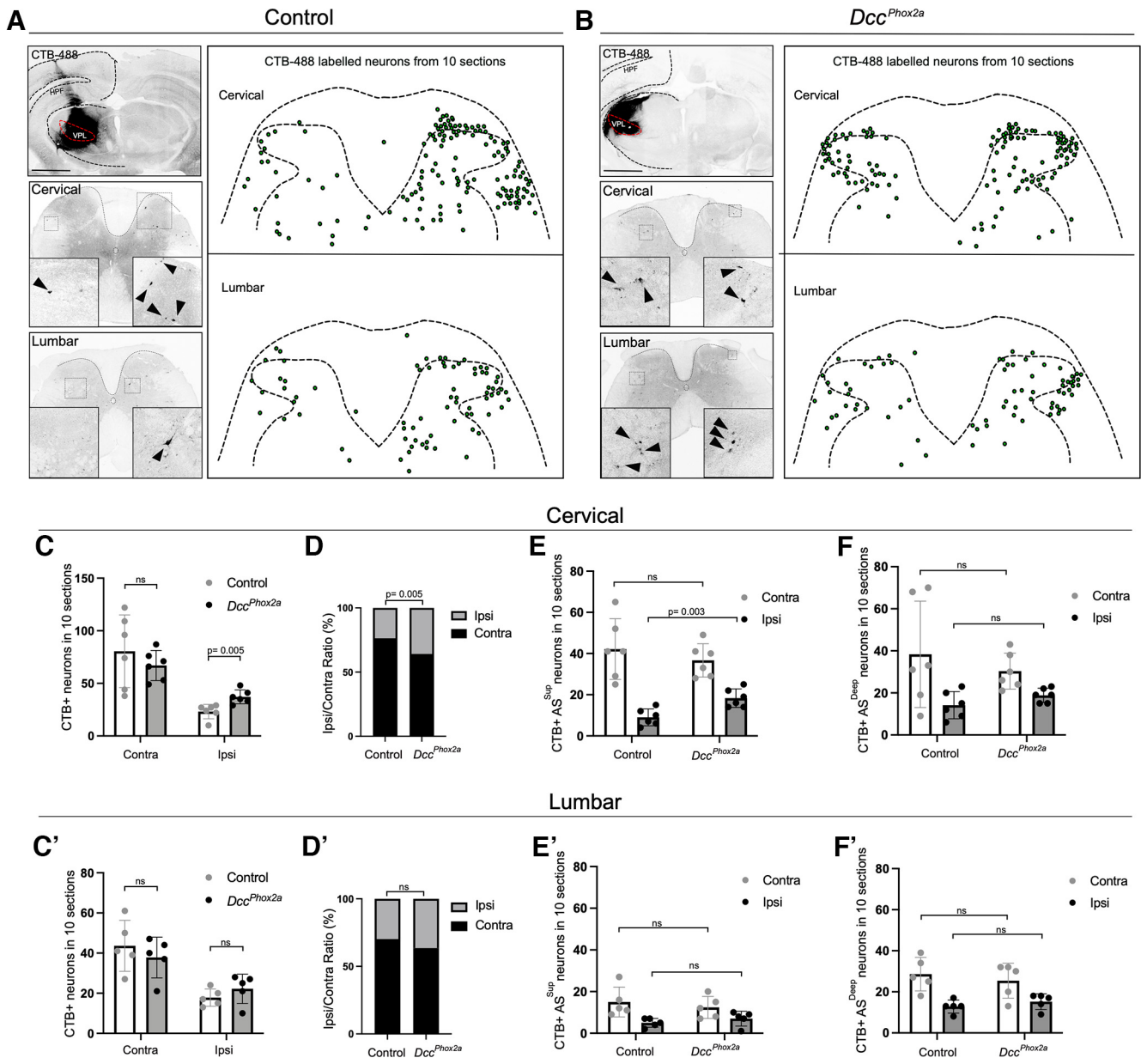

Figure 3. Increased ipsilateral innervation of the thalamus by AS neurons in Dcc^{Phox2a} mice. ***A***, ***B***, CTb-488 injection in adult control and Dcc^{Phox2a} VPL thalamus. Diagram illustrating the CTb-488 retrograde-labeled neurons in 10 nonsequential 25 μm sections of the cervical and lumbar spinal cord of one representative mouse. ***C***, ***C'***, Quantification of retrograde-labeled contralateral (contra) and ipsilateral (ipsi) Spinothalamic neurons. Total number of the neurons in 10 sections (25 μm) at cervical and lumbar spinal cord of the control and Dcc^{Phox2a} groups; $n = 6$ cervical and $n = 5$ lumbar groups; control contra, 80.5 $\pm$ 34.51; control ipsi, 23.16 $\pm$ 6.91; Dcc^{Phox2a} contra, 67 $\pm$ 14.26; Dcc^{Phox2a} ipsi, 37.16 $\pm$ 6.64 (***C***); control contra, 43.6 $\pm$ 12.72; control ipsi, 17.8 $\pm$ 4.32; Dcc^{Phox2a} contra, 37.8 $\pm$ 10.13; Dcc^{Phox2a} ipsi, 22.2 $\pm$ 7.32 (***C'***). Unpaired Student's *t* test; $p = 0.005$; significant; ns. Data indicate mean $\pm$ SD. ***D***, ***D'***, Percentage of ipsilateral versus contralateral thalamic projection neurons at cervical and lumbar spinal cord of the control and Dcc^{Phox2a} groups; $n = 6$ cervical and $n = 5$ lumbar groups; control contra, 76.37 $\pm$ 8.06%; control ipsi, 23.62 $\pm$ 8.06%; Dcc^{Phox2a} contra, 64.13 $\pm$ 2.34%; Dcc^{Phox2a} ipsi, 35.86 $\pm$ 2.34% (***D***); control contra, 70.2 $\pm$ 9.75%; control ipsi, 29.79 $\pm$ 9.75%; Dcc^{Phox2a} contra, 63.52 $\pm$ 3.16%; Dcc^{Phox2a} ipsi, 36.47 $\pm$ 3.16% (***D'***). Unpaired student's *t* test; $p = 0.005$; significant; ns. Data are represented as mean $\pm$ SD. ***E***, ***E'***, Number of CTb-488 tracer-labeled neurons in 10 sections (25 μm) of the cervical and lumbar AS^{Sup} neurons of control and Dcc^{Phox2a} mice; $n = 6$ cervical and $n = 5$ lumbar groups; control contra, 42.16 $\pm$ 14.75; control ipsi, 9 $\pm$ 4.09; Dcc^{Phox2a} contra, 36.66 $\pm$ 8.11; Dcc^{Phox2a} ipsi, 18.33 $\pm$ 4.5 (***E***); control contra, 15 $\pm$ 7.17; control ipsi, 5 $\pm$ 2.12; Dcc^{Phox2a} contra, 12.4 $\pm$ 5.32; Dcc^{Phox2a} ipsi, 7 $\pm$ 3.53 (***E'***). Unpaired student's *t* test; $p = 0.003$, significant; ns. Data indicate mean $\pm$ SD. ***F***, ***F'***, Number of CTb-488 tracer-labeled neurons in 10 sections (25 μm) of cervical and lumbar AS^{Deep} neurons of the control and Dcc^{Phox2a} mice; $n = 6$ cervical and $n = 5$ lumbar groups; control contra, 38.33 $\pm$ 25.29; control ipsi, 14.16 $\pm$ 6.49; Dcc^{Phox2a} contra, 30.33 $\pm$ 8.54; Dcc^{Phox2a} ipsi, 18.83 $\pm$ 3.37 (***F***); control contra, 28.6 $\pm$ 8.14; control ipsi, 12.8 $\pm$ 3.19; Dcc^{Phox2a} contra, 25.4 $\pm$ 8.53; Dcc^{Phox2a} ipsi, 15.2 $\pm$ 3.83 (***F'***). Unpaired Student's *t* test; ns. Data are represented as mean $\pm$ SD.

Cliffer et al., 1991). A small fraction of mCherry+ and GFP+ puncta overlapped in all three brain structures in control mice, which could be because of close apposition of lumbar and cervical axonal termini or the result of cervical AAV injections infecting some lumbar axons ascending through the neighboring white matter. The rate at which axonal termini were colabeled with mCherry and GFP did not differ among PB, PAG, and thalamus of control mice (6.67 $\pm$ 1.79%, 7.6 $\pm$ 2.88% and 7.62 $\pm$ 0.6%, respectively, not significant; Fig. 4*F*), suggesting that the signal overlap is likely because of coinfection artifacts. In general, in the lateral division of the PB and PAG of both groups of mice, lumbar and cervical AS axons were intermingled and not segregated to a particular target zone or biased in their distribution along rostrocaudal or mediolateral axes (Fig. 4*B*,*C*). The

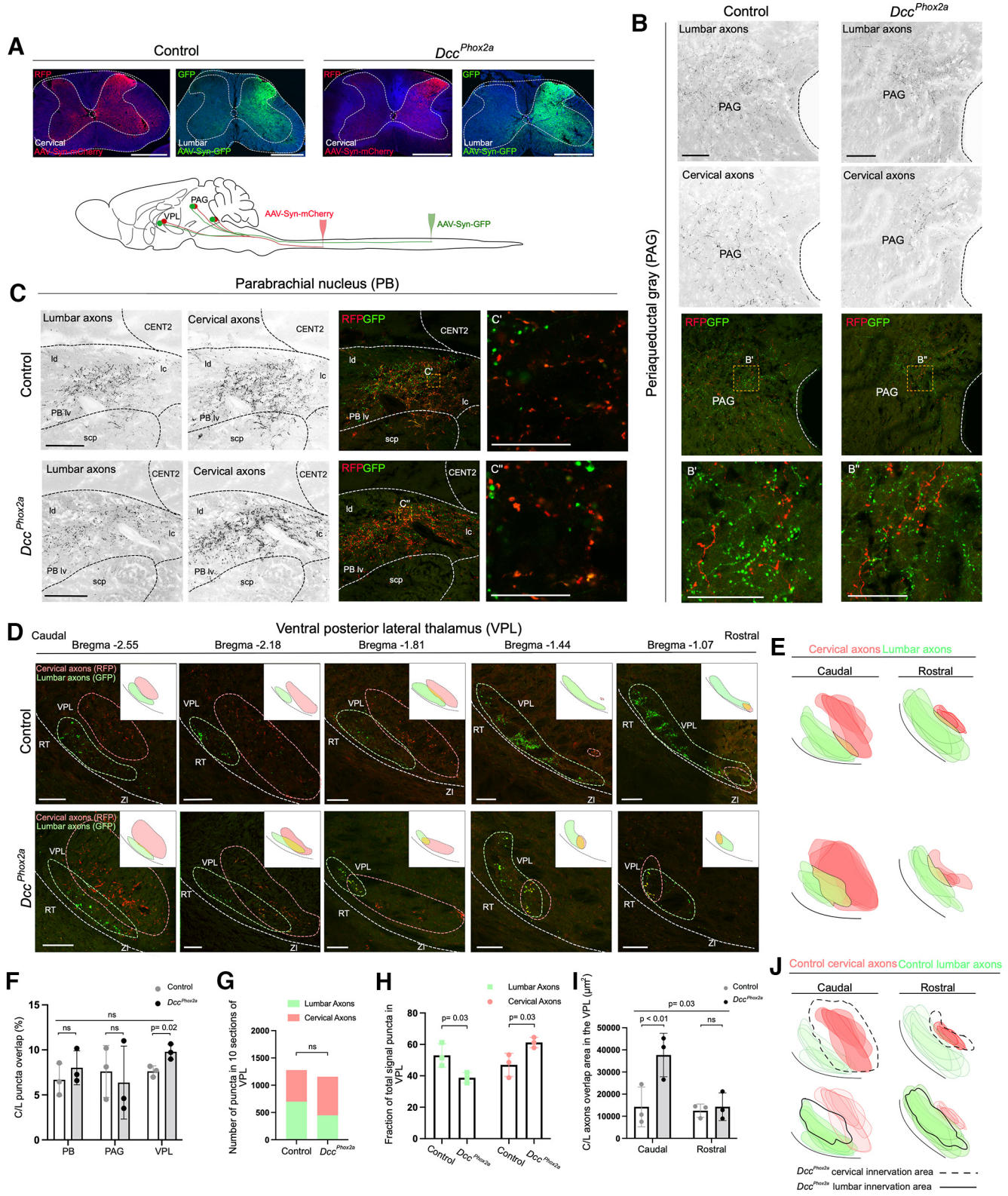

Figure 4. Impaired organization of spinothalamic innervation in Dcc^{Phox2a} mice. ***A***, Schematic of unilateral injection of AAV2/8-Syn-mCherry and AAV2/8-Syn-GFP in the cervical and lumbar spinal cord, respectively. mCherry and GFP expression was detected with anti-RFP and anti-GFP antibodies, respectively. ***B***, ***B′***, ***B″***, mCherry positive and GFP-positive axon terminals from, respectively, cervical and lumbar spinal cord in the PAG nucleus; $n = 3$ control and $n = 3$ Dcc^{Phox2a} mice. Scale bars: ***B***, 100 μm; ***B′***, ***B″***, 50 μm. ***C***, ***C′***, ***C″***, mCherry+ and GFP+ axon termini from, respectively, cervical and lumbar AS axons in the PB nucleus; $n = 3$ control and $n = 3$ Dcc^{Phox2a} mice. Scale bars: ***C***, 100 μm, 20× objective; ***C′***, ***C″***, 25 μm, 63× objective. ***D***, Five sequential sections from caudal to rostral VPL thalamus (−2.55 mm to −1.07 mm to bregma) in representative control and Dcc^{Phox2a} animals. mCherry+ (red) and GFP+ (green) AS axon terminals (puncta) represent the axon termini of the cervical and lumbar projection neurons, respectively. Scale bars: 100 μm. ***E***, Diagram of VPL areas innervated by cervical and lumbar AS neurons labeled with GFP and mCherry-expressing AAVs. The stacked outlines represent the innervation area of cervical/lumbar PNs averaged from three mice at five different levels relative to bregma, separated into rostral and caudal regions. Red outlines represent areas of cervical AS axon spread, green outlines represent the areas of lumbar AS axon spread, and yellow represents the overlap between the lumbar and cervical AS areas. In control mice the overlap is limited, whereas greater overlap is detected in Dcc^{Phox2a} mice (quantified in ***I***). ***F***, Fraction of axon terminal

rate of mCherry and GFP colabeling of axonal termini in the PB and PAG of Dcc^{Phox2a} was 8.01 ± 1.89% and 6.37 ± 4.04%, respectively, which was not significantly different from control mice ($p = 0.4$ and $p = 0.7$, respectively; Fig. 4*F*). Together, these observations suggest that lumbar and cervical termini in the PB and PAG were not somatotopically organized, a conclusion similar to the one made in the PB based on analogous AAV anterograde labeling (Choi et al., 2020).

Next, we considered lumbar and cervical AS axon innervation of the ventrobasal (VB) thalamus where electrophysiological characterization of neuronal receptive fields and other studies revealed a somatotopic organization in the VPL nucleus, previously implicated in nociception (Francis et al., 2008). Indeed, in the caudal VPL of three control animals, lumbar AS axons covered a territory located ventrolaterally relative to that occupied by cervical axons. In more rostral regions, essentially only lumbar axons were present in a similar ventrolateral location (Fig. 4*D*). Additionally, we found AS axons in the posterior limiting nucleus of the thalamus (PO), another VB region involved in nociception and potentially organized in a somatotopically manner, but this labeling was too sparse for a thorough analysis (Diamond et al., 1992; Frangeul et al., 2014; data not shown).

A qualitative mapping of the VPL territory covered by cervical and lumbar AS axon termini revealed that their somatotopic order was compromised in Dcc^{Phox2a} mice. In control animals, cervical axons terminated throughout the rostrocaudal extent of the VPL, and the territory covered by them only occasionally included lumbar axons in more rostral regions of the VPL (Fig. 4*D*, bregma −1.07). In the more caudal regions of the VPL, where the cervical and lumbar termini territories were consistently segregated in control animals, in Dcc^{Phox2a} mice we found many instances of lumbar axons present within the territory occupied by cervical axons (Fig. 4D, bregma −2.18 mm, −1.81 mm, etc.). This disordered arrangement was more evident when we superimposed the territories covered by cervical and lumbar axons from multiple caudal and rostral VPL sections, in three mice per genotype; although in controls these territories were mostly mutually exclusive, in Dcc^{Phox2a} mice many instances of cervical and lumbar axon territory overlap were evident (Fig. 4*E*, yellow shading).

Quantification of cervical and lumbar axon termini overlap and the VPL territories covered by them also revealed a compromised AS afferent organization. The frequency with which lumbar GFP and cervical mCherry axon terminal signal cosegregated within the VPL of control mice was similar to the frequency in Dcc^{Phox2a} and control PB and PAG (7.62 ± 0.6%; see above) but rose to 9.8 ± 0.84% in Dcc^{Phox2a} mice ($p = 0.02$; Fig. 4*F*). Furthermore, although the total amount of axon terminal signal in the VPL of Dcc^{Phox2a} and control mice did not differ significantly, the ratio of cervical to lumbar axon terminal signal increased in Dcc^{Phox2a} VPL in favor of cervical axons ($p = 0.03$; Fig. 4*G*,*H*). We also quantified the overlap between the territories covered by lumbar and cervical axons in Figure 4*E*, which revealed that it was significantly greater in Dcc^{Phox2a} mutants compared with controls (Fig. 4*I*). Finally, we estimated the territory covered by Dcc^{Phox2a} cervical and lumbar axons by overlaying them in three different animals and then comparing them to the VPL territory covered by control cervical and lumbar termini, a proxy for the location of the VPL neurons postsynaptic to them (Fig. 4*J*). This analysis revealed that Dcc^{Phox2a} cervical axon territory (stippled black outline) was larger than the control areas and extended into the control VPL regions subserved by lumbar axons, consistent with the observed number of cervical termini puncta (Fig. 4*H*). Similarly, we found that Dcc^{Phox2a} cervical axon territory (black outline) extended into the control VPL regions subserved by lumbar axons. Together, our results demonstrate that Dcc^{Phox2a} disrupts the normal organization of AS axons in the VPL with greater incidence of cosegregation of cervical and lumbar axons, instances of lumbar axons found in the VPL region normally innervated by cervical axons, and vice versa. This implies that VPL neurons normally subserved by cervical axons may receive lumbar projections in Dcc^{Phox2a} mutants.

Timeline of embryonic as neuron innervation of brain targets

The development of innervation of supraspinal targets by AS neurons is unknown, and the early stages of development of their targets are poorly characterized. To begin a dissection of the developmental mechanisms underlying the behavioral and anatomic phenotypes in Dcc^{Phox2a} mice, we next established a developmental timeline of Phox2a AS neuron innervation of the thalamus, PB, and the PAG. To do this, we monitored the progression of spinofugal axons originating from $Phox2a^{Cre}$ AS neurons using an axonal recombinase tdTomato reporter. We circumvented the developmental expression of $Phox2a^{Cre}$ in supraspinal regions by intersecting it with the spinal-cord-specific $Cdx2^{FlpO}$ driver and the Cre-FlpO recombinase-dependent tdTomato reporter ($R26^{FSF\text{-}LSL\text{-}tdT}$ or *Ai65*; Madisen et al., 2015), producing $Phox2a^{Cre}$; $Cdx2^{FlpO}$; $R26^{FSF\text{-}LSL\text{-}tdT/+}$ mice (Fig. 5*A*). This strategy was previously validated to exclude tdTomato expression from Phox2a-expressing supraspinal neurons (Roome et al., 2020). To determine the time of arrival of Phox2a AS axons in the developing ventrobasal thalamus and other nociceptive areas, we focused on development days E14.5, E15.5, and E16.5 and on postnatal day (P)2, based on previous timeline estimates (Davidson et al., 2010). The prosomeric model of thalamic development posits that the VB thalamus that contains the VPL and other AS neuron targets derives from the thalamic progenitor domain that expresses the transcription factor Sox2 (Vue et al., 2007). A neighboring

←

puncta colabeled with GFP and mCherry in three brain nuclei, PB, PAG and VPL thalamus; $n = 3$ control and $n = 3$ Dcc^{Phox2a} mice (control PB, 6.67 ± 1.78%; control PAG, 7.6 ± 2.88%; control VPL, 7.61 ± 0.6%; Dcc^{Phox2a} PB, 8.01 ± 1.89%; Dcc^{Phox2a} PAG, 6.37 ± 4.04%; Dcc^{Phox2a} VPL, 9.79 ± 0.84%). Between-subjects ANOVA was performed to compare three brain nuclei versus genotype; ns, Not significant. Unpaired Student's *t* test was performed to separately compare the control versus Dcc^{Phox2a} mice in each nucleus; $p = 0.02'$ significant; ns. Data indicate mean ± SD. ***G***, Total number of axon terminal signal puncta in the VPL, originating from lumbar (GFP+) and cervical (mCherry+) AS neurons; $n = 3$ control and $n = 3$ Dcc^{Phox2a} mice (control cervical axons, 578 ± 99.74; control lumbar axons, 699.66 ± 339.12; Dcc^{Phox2a} cervical axons, 707 ± 41.24; Dcc^{Phox2a} lumbar, 448 ± 36.75). Unpaired Student's *t* test; ns. Data indicate mean ± SD. ***H***, Proportion of cervical versus lumbar AS axon termini puncta as a fraction of all AS termini puncta in the VPL; $n = 3$ control and $n = 3$ Dcc^{Phox2a} mice (control cervical axons, 46.94 ± 7.45%; control lumbar axons, 53.05 ± 7.45%; Dcc^{Phox2a} cervical axons, 61.2 ± 3.31%; Dcc^{Phox2a} lumbar, 38.79 ± 3.31%). Unpaired Student's *t* test; $p = 0.03$; significant. Data indicate mean ± SD. ***I***, Overlap of cervical and lumbar axon terminals innervation area (μm^2) measured in five sequential sections of caudal and five sequential sections of rostral VPL in each animal; $n = 3$ control and $n = 3$ Dcc^{Phox2a} mice (control caudal VPL, 14 252 μm^2 ± 9013.99 μm^2; control rostral VPL, 12 502.325 μm^2 ± 2998.46 μm^2; Dcc^{Phox2a} caudal VPL, 37 684 μm^2 ± 9846.02 μm^2; Dcc^{Phox2a} rostral VPL, 14 304.18 μm^2 ± 6262.310 μm^2). Between-subject ANOVA with Bonferroni *post hoc* analysis; $p = 0.03$ and $p < 0.01$; significant; ns. Data indicate mean ± SD. ***J***, Diagram of altered innervation area of Dcc^{Phox2a} VPL cervical/lumbar map. Normal cervical and lumbar axons innervation areas from control mice are shown as red and green ovals, respectively. The area innervated by cervical AS axons in Dcc^{Phox2a} mutants is bound by a stippled line, and Dcc^{Phox2a} lumbar projection neurons (PNs) innervation is bound by a solid line.

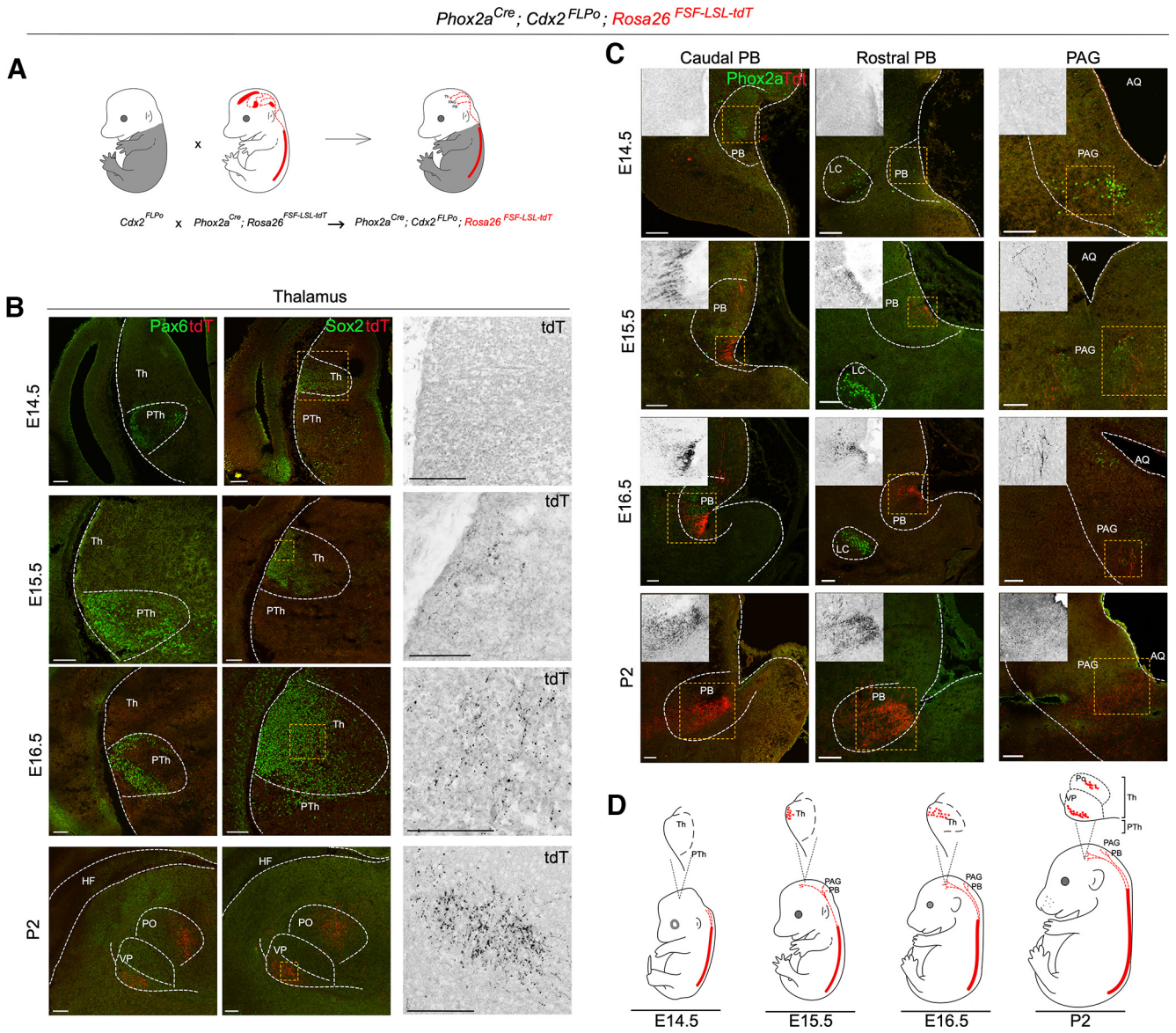

Figure 5. Development of Phox2a PNs projections from spinal cord to different brain targets. ***A***, Visualizing the *Phox2a*^{Cre} spinal specific axons by intersecting the *Phox2a*^{Cre} with spinal-cord-specific *Cdx2*^{Flp0} driver and the Cre-Flp0 recombinase-dependent tdTomato reporter (*R26*$^{FSF\text{-}LSL\text{-}tdT}$ or *Ai65*). This strategy has been used to specifically label spinal phox2a axons in the brain and trace them without labeling local axons in brain. ***B***, Phox2a-positive AS RFP positive axons arrival to the caudal and rostral PB as well as PAG at E14.5, E15.5, E16.5, and P2. Phox2a expression has been shown in proximity of spinal Phox2a axons. Also, Phox2a expression in the locus ceruleus (LC) as an anatomic landmark has been shown in rostral PB. TdT signal was boosted by tdT antibody; $n = 3$ control and $n = 3$ *Dcc*^{Phox2a} embryos. Scale bars: 100 μm. ***C***, Phox2a-positive PN axons arrival in the thalamus at E14.5, E15.5, E16.5, and P2. Sox2 and Pax6 have been used as Thalamus (Th) and prethalamus (PTh) markers, respectively. TdT signal was boosted by tdT antibody; $n = 3$ control and $n = 3$ *Dcc*^{Phox2a} embryos. Scale bars: 100 μm. ***D***, Diagram summarizing the pattern of Phox2a spinothalamic axons in E14.5, E15.5, E16.5, and P2.

ventral region named the prethalamus can be distinguished by the expression of the transcription factor Pax6 and eventually does not develop into any thalamic structures (Walther and Gruss, 1991; Nakagawa and O'Leary, 2001; Quintana-Urzainqui et al., 2020). Because the endogenous tdTomato expression in developing Phox2a AS axon termini was too weak to detect via its native fluorescence, we used an anti-tdTomato or anti-RFP antibody to localize it. At E14.5, one of the earliest ages at which the thalamus and prethalamus precursors can be distinguished molecularly, we did not detect any spinal Phox2a tdTomato-expressing axons in this region of the midbrain (Fig. 5*A*). At E15.5 the first tdTomato axons entered the lateral side of the Sox2-expressing thalamic domain. Between E15.5 and E16.5 this pattern expanded more medially within the Sox2 domain. In the P2 thalamus, the distribution of tdTomato-expressing axons was reminiscent of the adult pattern and included segregated PO and VPL domains (Fig. 5*B*).

To study the timing of innervation of the PB, we subdivided it via expression of Phox2a detected with an antibody (Pattyn et al., 1997). No Phox2a-derived AS axons were evident in the PB before E14.5, and the first tdTomato expressing axons reached it at the same time as the thalamus, at E15.5. Additional innervation of both rostral and caudal PB was detected at E16.5 and P2. As in the adult PB, Phox2a AS axons avoided Phox2a-expressing PB neurons in the medial division of the PB (Card et al., 2010). In contrast, Phox2a AS innervation of the PAG was evident as early as E14.5 when we found tdTomato axons in proximity of Phox2a PAG neurons (Fig. 5*C*). Together, this first genetic anterograde analysis of AS axonal development reveals the innervation of brain targets at a time when these

regions are still undergoing neurogenesis and early steps of molecular differentiation.

Expression of netrin-1 in the embryonic thalamus coincides with the arrival of AS axons

The disorganized AS axon innervation of the VPL in Dcc^{Phox2a} mutants and the impaired rostrocaudal localization of noxious stimuli raised the possibility that DCC functions not only in commissural crossing of AS axons but also by directing their innervation of the thalamus. We thus examined the expression of the DCC ligand netrin-1 in the thalamus at the time of its innervation by AS axons. As above, we used the expression of Sox2 to differentiate the precursors of the thalamus from the prethalamus. Thalamic netrin-1 protein was first detected at E15.5 in a Sox2-expressing region containing arriving tdTomato-expressing Phox2a AS axons (Fig. 6*A*; Powell et al., 2008). At this age, we also detected the expression of *Ntn1* mRNA in a region of the nascent thalamus more restricted than that of netrin-1 protein, as well as a more medially located ventricular zone region (Fig. 6*B*). This is consistent with previous observations that *Ntn1* mRNA and netrin-1 protein often do not coincide in their distribution (Kennedy et al., 2006; Varadarajan et al., 2017). At this age, we also examined embryos carrying the $Ntn1^{Bgeo}$ transgene, which is an insertion of a *lacZ* reporter gene in *Ntn1*, allowing us to use β-galactosidase as a proxy for *Ntn1* gene transcription (Skarnes et al., 1995). Analysis of E15.5 $Ntn1^{Bgeo}$ embryos revealed the presence of β-galactosidase in a pattern similar to that of *Ntn1* mRNA (Fig. 6*C*).

To determine whether AS axons express DCC protein at the time of target innervation, we examined its distribution in tdTomato-expressing AS axons in $Phox2a^{Cre}$; $Cdx2^{FlpO}$; $R26^{FSF\text{-}LSL\text{-}tdT/+}$ E15.5 embryos. First, we localized tdTomato-expressing axons in the dorsolateral aspect of the cervical spinal white matter, which in rodents is the site of many AS axons ascending toward their brain targets on the side contralateral to the location of AS neuron somata (Albe-Fessard et al., 1985; Hodge and Apkarian, 1990). Many of these coexpressed DCC protein suggesting that AS axons continue expressing DCC following their commissural crossing (Fig. 6*D*). Also, at E15.5, we detected DCC expression in the thalamus, with some of it coinciding with tdTomato, implying that although some DCC expression is endogenous to thalamic precursors, it is also present in afferent Phox2a AS axons (Fig. 6*E*,*E'*). Together, these observations raise the possibility that AS axons arriving in the thalamus detect netrin-1 protein through its receptor DCC.

Discussion

Our experiments demonstrate that selective genetic deletion of the netrin receptor DCC from mouse Phox2a neurons, many of which give rise to the pain-transmitting AS, results in aberrant development of connections between the spinal cord and thalamus. Dcc^{Phox2a} mice have an impaired ability to locate a noxious stimulus on the surface of their body but can appreciate its aversive nature. Our developmental and anatomic characterization of Dcc^{Phox2a} mice suggests a potential function of DCC in the somatotopic organization of AS neuron connections. We discuss these observations in the context of Phox2a AS neuron innervation of their brain targets and the role of AS neurons and their brain targets in nociception.

Development of AS neuron innervation of brain targets

Spinal commissural neurons have been the subject of many classical neurodevelopmental studies although relatively little is known about their development once their growth cones cross the midline and begin to grow toward the brain. Here, $Phox2a^{Cre}$ and a spinal FlpO transgene allowed us to anterogradely label a population of AS axons and determine that they arrive in the PB, PAG, and thalamus at approximately E15.5. This is earlier than previous estimates of the arrival of spinal afferents arrival based on retrograde tracing (Davidson et al., 2010), later than those based on classical anterograde labeling (Ding et al., 2003) but similar to the onset of trigeminothalamic innervation (Kivrak and Erzurumlu, 2013). Given that along with motor neurons, Phox2a AS neurons are the earliest born spinal neurons, their axonal extension timeline is consistent with the idea that neuronal birth time is inversely correlated with axonal length; the earlier a neuron is born, the farther its axon extends. Furthermore, the relatively early arrival of AS axons in the brain raises the intriguing possibility that they may be involved in directing the development of their target neurons. For example, the precocious presence of AS axons may allow them to participate in steps like postmitotic differentiation and sensory-experience-driven maturation of thalamic neurons, similar to the proposed role of trigeminothalamic axons (Ding et al., 2003; Kivrak and Erzurumlu, 2013).

DCC function in the laterality of Phox2a AS axon projections

Our previous work showed that deletion of DCC from the caudal spinal cord (Dcc^{SpC}) resulted a marked increase in the frequency of AS^{Sup} spinofugal axons innervating targets on the ipsilateral side (Da Silva et al., 2018; Bourojeni et al., 2021). Here, knocking out *Dcc* in Phox2a-expressing neurons results in a milder phenotype that is detected only at cervical levels, which could reflect a rostrocaudal bias in the onset of $Phox2a^{Cre}$ expression with respect to midline crossing; both events occur soon after birth of Phox2a neurons. Also, because Phox2a is not expressed in adult neurons, we could not directly assess the laterality of Phox2a AS neurons and relied on tracing experiments, whose interpretation is confounded by the proportion of developing AS neurons expressing $Phox2a^{Cre}$. Our previous analyses suggest that $Phox2a^{Cre}$ is expressed in ~50% of AS^{Sup} neurons, which combined with their paucity at lumbar levels (Davidson et al., 2010) means that subtle laterality changes in Phox2a AS neurons might not be revealed at the level of the whole AS^{Sup} population in the lumbar spinal cord. Given that only ~10% of AS^{Deep} neurons express $Phox2a^{Cre}$, and that most of these neurons have an ipsilateral anatomy, it is not surprising that Dcc^{Phox2a} does not significantly change the laterality of AS^{Deep} neurons. Neogenin, another netrin receptor widely expressed in the spinal cord and functionally redundant with DCC in commissural guidance, might contribute to the limited magnitude of AS axon crossing phenotypes in Dcc^{Phox2a} mice (Keino-Masu et al., 1996; Xu et al., 2014).

DCC function in the development of thalamic maps?

Our experiments suggest a potential function for DCC in AS axon guidance following spinal midline crossing. DCC protein is distributed along embryonic AS axons in the lateral spinal white matter and on those arriving in the VB thalamus. Intriguingly, at this time, *Ntn1* is also expressed in the developing VB thalamus. The nature of defects in the organization of afferent AS axons in the VPL of Dcc^{Phox2a} mice hints at a potential netrin-1:DCC function there. One principal phenotype is the increased VPL territory covered by cervical axons and lumbar axons reaching the VPL region that is normally innervated by cervical axons. A

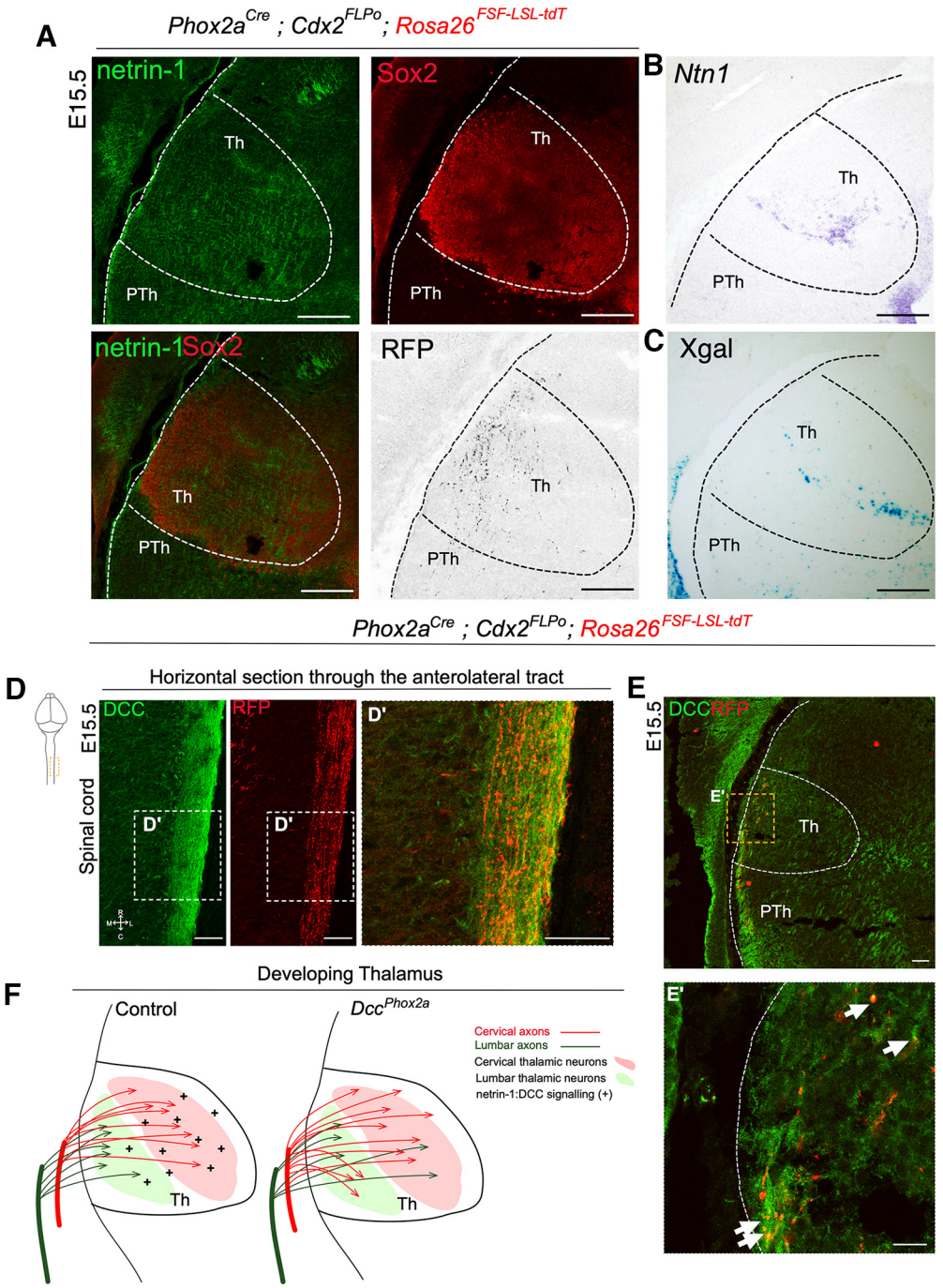

Figure 6. Role of netrin-1:DCC signaling in shaping the somatotopic order within embryonic thalamus. ***A***, Netrin-1 immunofluorescence in an E15.5 *Phox2a*^{Cre}; *Cdx2*^{FlpO}; *R26*$^{FSF\text{-}LSL\text{-}tdT/+}$ thalamus in proximity to Phox2a AS RFP+ axons. Sox2 protein has been used as an embryonic thalamic marker. Coronal sections, 25 μm thick, were used to assess the distribution of netrin-1 protein and Phox2a AS RFP +ve axons in the neighboring sections; $n = 3$ control and $n = 3$ *Dcc*^{Phox2a} embryos. Scale bars: 100 μm. ***B***, *In situ* hybridization detection of *Ntn1* mRNA in E15.5 thalamus; $n = 3$ control and $n = 3$ *Dcc*^{Phox2a} embryos. Scale bar: 100 μm. ***C***, X-gal staining in *Ntn1*^{Bgeo} mice reveals *Ntn1* expression in the thalamus of E15.5 embryos; $n = 3$ control and $n = 3$ *Dcc*^{Phox2a} embryos. Scale bar: 100 μm. ***D***, ***D′***, A horizontal section through the anterolateral tract showing Phox2a AS axons (RFP positive) expressing DCC at E15.5; $n = 3$ control and $n = 3$ *Dcc*^{Phox2a} embryos. Scale bar: 100 μm. ***E***, ***E′***, Phox2a AS axons (RFP positive) express DCC in the developing thalamus at E15.5. Arrowheads indicate colocalization of DCC and RFP; $n = 3$ control and $n = 3$ *Dcc*^{Phox2a} embryos. Scale bar: 100 μm. ***F***, Model of cervical and lumbar AS axon organization within the developing thalamus and how the lack of netrin-1:DCC signaling might change the map in *Dcc*^{Phox2a} mice.

precedent for deficient thalamic afferent organization was found in mice in which trigeminothalamic axons that lack Robo3 result in increased frequency of innervation of the ipsilateral ventral posteriomedial thalamus (Renier et al., 2017). This results in segregated domains of ipsilateral and contralateral trigeminal axons organized into barrel fields with preserved somatotopy. Our anatomic analysis did not reveal such arrangements of AS axons in the VPL of *Dcc*^{Phox2a} mice. Furthermore, our behavioral analyses do not reveal any significant left-right stimulus localization defects but do demonstrate deficient stimulus localization along the rostrocaudal axis. Given the small magnitude of the spinal commissure crossing phenotypes, an alternative explanation might be that the defective distribution of AS afferents in the VPL reflect a DCC function in thalamic innervation. For

example, given its role as an extracellular adhesion molecule that promotes synaptogenesis (Goldman et al., 2013), thalamic netrin-1 protein might promote increased AS axon adhesion. Thus, in Dcc^{Phox2a} mutants, because of decreased netrin-1: DCC adhesive signaling, cervical AS axons spread beyond their normal VPL target area, and lumbar AS axons terminate in VPL areas normally subserved by cervical axons (Fig. 6*F*). Intriguingly, a netrin-1 gradient has been previously evoked in the development of ordered neuronal maps (Shatzmiller et al., 2008; Li et al., 2014).

Insights into neuronal circuits mediating topognosis

In contrast to Dcc^{SpC} mutants, which display left-right side discrimination deficits, Dcc^{Phox2a} mutants lick their forelimbs in response to hindlimb stimulation, with relatively few left-right discrimination errors. How can these behaviors be linked to defective AS neuron anatomy and connectivity? We previously demonstrated that DCC is required for the dorsal horn positioning of Phox2a AS neurons (Roome et al., 2022); however, our data suggest this function is transient and related to the positioning of AS^{Sup} neurons along the mediolateral axis of the dorsal horn, associated with the proximo-distal dimension of limb somatotopy (Levinsson et al., 2002). The stimulus localization errors observed in Dcc^{Phox2a} mutants are along the rostrocaudal axis and are consistent with lumbar AS axons terminating in VPL regions normally subserved by cervical axons, which would result in cervical VPL neurons being activated by lumbar stimuli.

More generally, the VPL innervation defects observed in Dcc^{Phox2a} mutants raise the question of the identity of the neural circuits concerned with the location of noxious stimuli. Within the spinal cord, past experiments assigned a discriminatory function to AS^{Sup} neurons based on their modality-specific activation, small receptive fields, and connectivity, contrasting the emotive/motivational function assigned to AS^{Deep} neurons (Price and Dubner, 1977). $Phox2a^{Cre}$ expression is also more biased toward AS^{Sup} neurons compared with AS^{Deep} neurons, meaning that DCC loss would principally affect the development of AS^{Sup} neurons and have a minimal impact on the emotive dimension of nociception, consistent with our conditioned place aversion data. The function in stimulus localization of AS neuron brain targets is less clear. A somatotopic organization of afferent termini carrying information related to stimulus location on the surface of the body is a logical prerequisite for such a function. Our anterograde tracing experiments, and those of others failed to uncover an ordered arrangement of AS axons in the PB or the PAG (Bernard et al., 1995; Raboisson et al., 1996; Choi et al., 2020). One thalamic region with evidence of somatotopic organization and nociceptive function is the PO (Diamond et al., 1992; Frangeul et al., 2014); however, because of anterograde labeling limitations we were not able to assess its development and innervation in Dcc^{Phox2a} mutants. Our anterograde tracing experiment, which is not specific to Phox2a AS axons, is in line with electrophysiological recordings that reveal a somatotopic organization of VPL neurons (Francis et al., 2008). The aberrant VPL distribution of spinothalamic cervical and lumbar axons correlates with defective localization of a noxious stimulus by Dcc^{Phox2a} mice and suggests that this thalamic subnucleus may participate in nociceptive topognosis. A more precise functional experiment is required to eventually differentiate the contribution of the VPL and PO to nociception.

References

Abraira VE, et al. (2017) The cellular and synaptic architecture of the mechanosensory dorsal horn. Cell 168:295–310.e219.

Albe-Fessard D, Berkley KJ, Kruger L, Ralston HJ 3rd, Willis WD Jr (1985) Diencephalic mechanisms of pain sensation. Brain Res 356:217–296.

Alsulaiman WAA, Quillet R, Bell AM, Dickie AC, Polgár E, Boyle KA, Watanabe M, Roome RB, Kania A, Todd AJ, Gutierrez-Mecinas M (2021) Characterisation of lamina I anterolateral system neurons that express Cre in a Phox2a-Cre mouse line. Sci Rep 11:17912.

Bernard JF, Dallel R, Raboisson P, Villanueva L, Le Bars D (1995) Organization of the efferent projections from the spinal cervical enlargement to the parabrachial area and periaqueductal gray: a PHA-L study in the rat. J Comp Neurol 353:480–505.

Bernard JF, Bester H, Besson JM (1996) Involvement of the spino-parabrachio -amygdaloid and -hypothalamic pathways in the autonomic and affective emotional aspects of pain. Prog Brain Res 107:243–255.

Bourojeni FB, Zeilhofer HU, Kania A (2021) Netrin-1 receptor DCC is required for the contralateral topography of lamina I anterolateral system neurons. Pain 162:161–175.

Card JP, Lois J, Sved AF (2010) Distribution and phenotype of Phox2a-containing neurons in the adult sprague-dawley rat. J Comp Neurol 518:2202–2220.

Chaplan SR, Bach FW, Pogrel JW, Chung JM, Yaksh TL (1994) Quantitative assessment of tactile allodynia in the rat paw. J Neurosci Methods 53:55–63.

Chiang MC, Bowen A, Schier LA, Tupone D, Uddin O, Heinricher MM (2019) Parabrachial complex: a hub for pain and aversion. J Neurosci 39:8225–8230.

Choi S, Hachisuka J, Brett MA, Magee AR, Omori Y, Iqbal NU, Zhang D, DeLisle MM, Wolfson RL, Bai L, et al. (2020) Parallel ascending spinal pathways for affective touch and pain. Nature 587:258–263.

Cliffer KD, Burstein R, Giesler GJ Jr (1991) Distributions of spinothalamic, spinohypothalamic, and spinotelencephalic fibers revealed by anterograde transport of PHA-L in rats. J Neurosci 11:852–868.

Comer JD, Alvarez S, Butler SJ, Kaltschmidt JA (2019) Commissural axon guidance in the developing spinal cord: from Cajal to the present day. Neural Dev 14:9.

Cunningham CL, Gremel CM, Groblewski PA (2006) Drug-induced conditioned place preference and aversion in mice. Nat Protoc 1:1662–1670.

Da Silva RV, Johannssen HC, Wyss MT, Roome RB, Bourojeni FB, Stifani N, Marsh APL, Ryan MM, Lockhart PJ, Leventer RJ, Richards LJ, Rosenblatt B, Srour M, Weber B, Zeilhofer HU, Kania A (2018) DCC is required for the development of nociceptive topognosis in mice and humans. Cell Rep 22:1105–1114.

Davidson S, Truong H, Giesler GJ Jr (2010) Quantitative analysis of spinothalamic tract neurons in adult and developing mouse. J Comp Neurol 518:3193–3204.

Diamond ME, Armstrong-James M, Ebner FF (1992) Somatic sensory responses in the rostral sector of the posterior group (POm) and in the ventral posterior medial nucleus (VPM) of the rat thalamus. J Comp Neurol 318:462–476.

Ding YQ, Yin J, Xu HM, Jacquin MF, Chen ZF (2003) Formation of whisker-related principal sensory nucleus-based lemniscal pathway requires a paired homeodomain transcription factor, Drg11. J Neurosci 23:7246–7254.

Fazeli A, Dickinson SL, Hermiston ML, Tighe RV, Steen RG, Small CG, Stoeckli ET, Keino-Masu K, Masu M, Rayburn H, Simons J, Bronson RT, Gordon JI, Tessier-Lavigne M, Weinberg RA (1997) Phenotype of mice lacking functional Deleted in colorectal cancer (Dcc) gene. Nature 386:796–804.

Francis JT, Xu S, Chapin JK (2008) Proprioceptive and cutaneous representations in the rat ventral posterolateral thalamus. J Neurophysiol 99:2291–2304.

Frangeul L, Porrero C, Garcia-Amado M, Maimone B, Maniglier M, Clascá F, Jabaudon D (2014) Specific activation of the paralemniscal pathway during nociception. Eur J Neurosci 39:1455–1464.

Geiger BM, Frank LE, Caldera-Siu AD, Pothos EN (2008) Survivable stereotaxic surgery in rodents. J Vis Exp 2008:880.

Goldman JS, Ashour MA, Magdesian MH, Tritsch NX, Harris SN, Christofi N, Chemali R, Stern YE, Thompson-Steckel G, Gris P, Glasgow SD, Grutter P, Bouchard JF, Ruthazer ES, Stellwagen D, Kennedy TE (2013)

Netrin-1 promotes excitatory synaptogenesis between cortical neurons by initiating synapse assembly. J Neurosci 33:17278–17289.
Hargreaves K, Dubner R, Brown F, Flores C, Joris J (1988) A new and sensitive method for measuring thermal nociception in cutaneous hyperalgesia. Pain 32:77–88.
Hodge CJ Jr., Apkarian AV (1990) The spinothalamic tract. Crit Rev Neurobiol 5:363–397.
Huang T, Lin SH, Malewicz NM, Zhang Y, Zhang Y, Goulding M, LaMotte RH, Ma Q (2019) Identifying the pathways required for coping behaviours associated with sustained pain. Nature 565:86–90.
Hunt SP, Pini A, Evan G (1987) Induction of c-*fos*-like protein in spinal cord neurons following sensory stimulation. Nature 328:632–634.
Karthik S, Huang D, Delgado Y, Laing JJ, Peltekian L, Iverson GN, Grady F, Miller RL, McCann CM, Fritzsch B, Iskusnykh IY, Iskusnykh IY, Geerling JC (2022) Molecular ontology of the parabrachial nucleus. J Comp Neurol 530:1658–1699.
Keino-Masu K, Masu M, Hinck L, Leonardo ED, Chan SS, Culotti JG, Tessier-Lavigne M (1996) Deleted in Colorectal Cancer (DCC) encodes a netrin receptor. Cell 87:175–185.
Kennedy TE, Serafini T, de la Torre JR, Tessier-Lavigne M (1994) Netrins are diffusible chemotropic factors for commissural axons in the embryonic spinal cord. Cell 78:425–435.
Kennedy TE, Wang H, Marshall W, Tessier-Lavigne M (2006) Axon guidance by diffusible chemoattractants: a gradient of netrin protein in the developing spinal cord. J Neurosci 26:8866–8874.
Kivrak BG, Erzurumlu RS (2013) Development of the principal nucleus trigeminal lemniscal projections in the mouse. J Comp Neurol 521:299–311.
Kohro Y, Sakaguchi E, Tashima R, Tozaki-Saitoh H, Okano H, Inoue K, Tsuda M (2015) A new minimally-invasive method for microinjection into the mouse spinal dorsal horn. Sci Rep 5:14306.
Krimpenfort P, Song JY, Proost N, Zevenhoven J, Jonkers J, Berns A (2012) Deleted in colorectal carcinoma suppresses metastasis in p53-deficient mammary tumours. Nature 482:538–541.
Lein ES, et al. (2007) Genome-wide atlas of gene expression in the adult mouse brain. Nature 445:168–176.
Levinsson A, Holmberg H, Broman J, Zhang M, Schouenborg J (2002) Spinal sensorimotor transformation: relation between cutaneous somatotopy and a reflex network. J Neurosci 22:8170–8182.
Li J, Duarte T, Kocabas A, Works M, McConnell SK, Hynes MA (2014) Evidence for topographic guidance of dopaminergic axons by differential Netrin-1 expression in the striatum. Mol Cell Neurosci 61:85–96.
Lima D (2008) Ascending pathways: anatomy and physiology. In Science of pain (Basbaum AI, Bushnell MC, eds), pp 477–526. Boston: Elsevier.
Madisen L, Zwingman TA, Sunkin SM, Oh SW, Zariwala HA, Gu H, Ng LL, Palmiter RD, Hawrylycz MJ, Jones AR, Lein ES, Zeng H (2010) A robust and high-throughput Cre reporting and characterization system for the whole mouse brain. Nat Neurosci 13:133–140.
Madisen L, et al. (2015) Transgenic mice for intersectional targeting of neural sensors and effectors with high specificity and performance. Neuron 85:942–958.
Mogil JS, Graham AC, Ritchie J, Hughes SF, Austin J-S, Schorscher-Petcu A, Langford DJ, Bennett GJ (2010) Hypolocomotion, asymmetrically directed behaviors (licking, lifting, flinching, and shaking) and dynamic weight bearing (gait) changes are not measures of neuropathic pain in mice. Mol Pain 6:34.
Nakagawa Y, O'Leary DD (2001) Combinatorial expression patterns of LIM-homeodomain and other regulatory genes parcellate developing thalamus. J Neurosci 21:2711–2725.
Oh SW, et al. (2014) A mesoscale connectome of the mouse brain. Nature 508:207–214.
Pattyn A, Morin X, Cremer H, Goridis C, Brunet JF (1997) Expression and interactions of the two closely related homeobox genes Phox2a and Phox2b during neurogenesis. Development 124:4065–4075.
Pilyavskii AI, Maznychenko AV, Maisky VA, Kostyukov AI, Hellström F, Windhorst U (2005) Capsaicin-induced effects on c-fos expression and NADPH-diaphorase activity in the feline spinal cord. Eur J Pharmacol 521:70–78.
Powell AW, Sassa T, Wu Y, Tessier-Lavigne M, Polleux F (2008) Topography of thalamic projections requires attractive and repulsive functions of Netrin-1 in the ventral telencephalon. PLoS Biol 6:e116.
Price DD, Dubner R (1977) Neurons that subserve the sensory-discriminative aspects of pain. Pain 3:307–338.
Quintana-Urzainqui I, Hernández-Malmierca P, Clegg JM, Li Z, Kozić Z, Price DJ (2020) The role of the diencephalon in the guidance of thalamocortical axons in mice. Development 147
Raboisson P, Dallel R, Bernard JF, Le Bars D, Villanueva L (1996) Organization of efferent projections from the spinal cervical enlargement to the medullary subnucleus reticularis dorsalis and the adjacent cuneate nucleus: a PHA-L study in the rat. J Comp Neurol 367:503–517.
Renier N, Dominici C, Erzurumlu RS, Kratochwil CF, Rijli FM, Gaspar P, Chédotal A (2017) A mutant with bilateral whisker to barrel inputs unveils somatosensory mapping rules in the cerebral cortex. Elife 6: e2349.
Rexed B (1952) The cytoarchitectonic organization of the spinal cord in the cat. J Comp Neurol 96:414–495.
Ribeiro-da-Silva A, De Koninck Y (2008) Morphological and neurochemical organization of the spinal dorsal horn. In Science of pain (Basbaum AI, Bushnell MC, eds), pp 279–310. Boston: Elsevier.
Roome RB, Bourojeni FB, Mona B, Rastegar-Pouyani S, Blain R, Dumouchel A, Salesse C, Thompson WS, Brookbank M, Gitton Y, Tessarollo L, Goulding M, Johnson JE, Kmita M, Chédotal A, Kania A (2020) Phox2a defines a developmental origin of the anterolateral system in mice and humans. Cell Rep 33:108425.
Roome RB, Rastegar-Pouyani S, Ker A, Dumouchel A, Kmita M, Kania A (2022) Netrin1 and reelin signaling are required for the migration of anterolateral system neurons in the embryonic spinal cord. Pain 163:e527–e539.
Rozen S, Skaletsky H (2000) Primer3 on the WWW for general users and for biologist programmers. Methods Mol Biol 132:365–386.
Sakurada T, Katsumata K, Tan-No K, Sakurada S, Kisara K (1992) The capsaicin test in mice for evaluating tachykinin antagonists in the spinal cord. Neuropharmacology 31:1279–1285.
Schneider CA, Rasband WS, Eliceiri KW (2012) NIH Image to ImageJ: 25 years of image analysis. Nat Methods 9:671–675.
Serafini T, Colamarino SA, Leonardo ED, Wang H, Beddington R, Skarnes WC, Tessier-Lavigne M (1996) Netrin-1 is required for commissural axon guidance in the developing vertebrate nervous system. Cell 87:1001–1014.
Shatzmiller RA, Goldman JS, Simard-Emond L, Rymar V, Manitt C, Sadikot AF, Kennedy TE (2008) Graded expression of netrin-1 by specific neuronal subtypes in the adult mammalian striatum. Neuroscience 157:621–636.
Skarnes WC, Moss JE, Hurtley SM, Beddington RS (1995) Capturing genes encoding membrane and secreted proteins important for mouse development. Proc Natl Acad Sci U S A 92:6592–6596.
Tessier-Lavigne M, Placzek M, Lumsden AG, Dodd J, Jessell TM (1988) Chemotropic guidance of developing axons in the mammalian central nervous system. Nature 336:775–778.
Tiveron M-C, Hirsch M, Brunet J-F (1996) The expression pattern of the transcription factor Phox2 delineates synaptic pathways of the autonomic nervous system. J Neusci 16:7649–7660.
Todd AJ (2010) Neuronal circuitry for pain processing in the dorsal horn. Nat Rev Neurosci 11:823–836.
Tzschentke TM (2014) Conditioned place preference and aversion. In Encyclopedia of Psychopharmacology 1–7. Available at https://link.springer.com/referenceworkentry/10.1007/978-3-642-27772-6_146-2.
Varadarajan SG, Kong JH, Phan KD, Kao TJ, Panaitof SC, Cardin J, Eltzschig H, Kania A, Novitch BG, Butler SJ (2017) Netrin1 produced by neural progenitors, not floor plate cells, is required for axon guidance in the spinal cord. Neuron 94:790–799.e3.
Vue TY, Aaker J, Taniguchi A, Kazemzadeh C, Skidmore JM, Martin DM, Martin JF, Treier M, Nakagawa Y (2007) Characterization of progenitor domains in the developing mouse thalamus. J Comp Neurol 505:73–91.
Walther C, Gruss P (1991) Pax-6, a murine paired box gene, is expressed in the developing CNS. Development 113:1435–1449.
Wercberger R, Braz JM, Weinrich JA, Basbaum AI (2021) Pain and itch processing by subpopulations of molecularly diverse spinal and trigeminal projection neurons. Proc Natl Acad Sci U S A 118:e2105732118.
Xu K, Wu Z, Renier N, Antipenko A, Tzvetkova-Robev D, Xu Y, Minchenko M, Nardi-Dei V, Rajashankar KR, Himanen J, Tessier-Lavigne M, Nikolov DB (2014) Neural migration. Structures of netrin-1 bound to two receptors provide insight into its axon guidance mechanism. Science 344:1275–1279.